석 사 학 위 논 문

Master's Thesis

구조 동역학 해석을 위한 다중 레벨 부구조화법 기반 모델축소기법의 개선

Improving the model reduction method based on multilevel substructuring for structural dynamic analysis

2018

현 철 규 (玄 喆 奎 Hyun, Cheolgyu)

한 국 과 학 기 술 원

Korea Advanced Institute of Science and Technology

석 사 학 위 논 문

구조 동역학 해석을 위한 다중 레벨 부구조화법 기반 모델축소기법의 개선

2018

현 철 규

한 국 과 학 기 술 원

기계항공공학부 기계공학과

구조 동역학 해석을 위한 다중 레벨 부구조화법 기반 모델축소기법의 개선

현 철 규

위 논문은 한국과학기술원 석사학위논문으로
학위논문 심사위원회의 심사를 통과하였음

2017년 12월 11일

심사위원장 이 필 승 (인)

심 사 위 원 박 용 화 (인)

심 사 위 원 정 형 조 (인)

Improving the model reduction method based on multilevel substructuring for structural dynamic analysis

Cheolgyu Hyun

Advisor: Phill-Seung Lee

A thesis submitted to the faculty of
Korea Advanced Institute of Science and Technology in
partial fulfillment of the requirements for the degree of
Master of Science in Mechanical Engineering

Daejeon, Korea
December 11, 2017

Approved by

Phill-Seung Lee
Professor of Mechanical Engineering

The study was conducted in accordance with Code of Research Ethics[1)].

1) Declaration of Ethical Conduct in Research**:** I, as a graduate student of Korea Advanced Institute of Science and Technology, hereby declare that I have not committed any act that may damage the credibility of my research. This includes, but is not limited to, falsification, thesis written by someone else, distortion of research findings, and plagiarism. I confirm that my dissertation contains honest conclusions based on my own careful research under the guidance of my advisor.

MME 20163698

현철규. 구조 동역학 해석을 위한 다중 레벨 부구조화법 기반 모델축소기법의 개선. 기계항공공학부 기계공학과. 2018년. 55+iii 쪽. 지도교수: 이필승. (영문 논문)

Cheolgyu Hyun. Improving the model reduction method based on multilevel substructuring for structural dynamic analysis. School of Mechanical and Aerospace Engineering, Department of Mechanical Engineering. 2018. 55+iii pages. Advisor: Phill-Seung Lee. (Text in English)

초 록

본 논문에서는 enhanced automated multilevel substructuring method (EAMLS)의 새로운 수식을 제시한다. 전산 효율성을 개선시키기위해 많은 전산 시간과 컴퓨터 메모리를 요구하는 문제들을 확인하고 효과적인 조치를 취했다. 새로운 수식에서는 축소된 상위 레벨 부구조들(Higher level substructure)를 조립(Assemble)해 확장된 루트 부구조(Extended root substructure)를 정의하고, 이를 이용해 유도된 정제된 부분공간(Refined subspace)위로 축소 모델을 사영(Projection)시킨다. 그런 다음, 하부 레벨 부구조(Bottom level substructure)의 잔류 유연도 행렬(Residual flexibility matrix)로 계산된 잔류 부구조 모드 보정(Residual substructural modes correction)은 질량 행렬에 대해서만 수행되는데, 이는 계산 비용 및 필요 메모리의 감소효과를 가져온다. 또한 축소된 질량 및 강성 행렬은 전역 행렬(Global matrix)이 아닌 부분 행렬(Submatrix) 단위에서 계산된다. 새로운 수식의 정확도와 전산 효율성은 여러가지 대형 유한요소 모델을 통해 입증하였다.

핵 심 낱 말 구조 동역학, 유한요소법, 모델 축소, 부분 구조 합성법, AMLS 기법, 고유치 문제

Abstract

In this thesis, a new formulation of the enhanced automated multilevel substructuring method (EAMLS) is presented. To improve the computational efficiency, the major problems which required large computation time and computer memory are inspected and dealt with effectively. In the new formulations, an extended root substructure is defined by assembling the reduced higher level substructures, and reduced model is projected on a new refined subspace derived by extended root substructure. Then, the residual substructural modes correction computed by residual flexibility matrices of bottom substructures is performed only for the mass matrix, which gives rise to reduction of computational cost and required memory. In addition, the reduced mass and stiffness matrices are computed by submatrix level instead of global matrix. The solution accuracy and computational efficiency of the new formulation are demonstrated through several large FE models.

Keywords Structural dynamics, Finite element method, Model reduction, Component mode synthesis, Automated multilevel substructuring method, Eigenvalue problem

Contents

List of Tables

List of Figures

Chapter 1. Introduction

1.1 Background

In recent years, there has been an increasing demand of using the finite element method (FEM) [1] for dynamic response analysis of large and complex structures such as automobiles, airplanes and ships. In spite of enormous improvement of computer performance, considerable computation time is required for dynamic analysis of large finite element (FE) model since the FE model of these structures has more than several million degrees of freedom (DOFs). In order to alleviate this inconvenience, simplified FE model is essential for computational efficiency and thus the model reduction methods have been emerged from many engineering fields [2-36]. In the field of structural dynamics, the model reduction methods can distinguish two major category: physical coordinate reduction referred to condensation and generalized coordinate reduction.

In condensation method, DOFs of the global FE model are divided into master DOFs and slave DOFs, and the inertial effect and stiffness of the slave DOFs are condensed in the master DOFs. Condensation methods can be categorized as static and dynamic condensation depending on handling inertial effect. Static condensation, first proposed by Guyan [2] and Irons [3] in 1965, ignore the inertial effect completely. Thus, the solution accuracy is guaranteed for only static or low frequency modes. To resolve this limitation, dynamic condensation an improved method of static condensation by considering the inertial effect properly was proposed [4–10]. These methods have been widely used due to its simple implementation and solution accuracy.

Typically, coordinates which are not physical coordinates indicate the generalized coordinates including but not limited to modal coordinates. Modal coordinate reduction, referred to modal superposition or mode superposition, is one of the representative methods of the generalized coordinate reduction. Mode superposition method is the method of projecting the response of the system to finite number of normal modes such as mode displacement, mode acceleration. When it is difficult to solve the eigenvalue problem due to the large size of the FE model, a reduced mass and stiffness matrices which are made by component mode synthesis (CMS) can be used. The CMS, first proposed by Hurty [11], is related to domain decomposition method that divides structure into many substructures. A global (original) FE model is decomposed into several substructures, eigenvalue problems for each substructure are solved, and a reduced model is constructed by using dominant substructural modes. Craig and Bampton simplify the Hurty's method, which is the most popular method in CMS called Craig-Bampton (CB) method [12] and has been widely used. Over the decades, various studies on CMS have been carried out [13–29].

1.2 Motivation and objective

The automated multilevel substructuring (AMLS) method [15–17] is an efficient model reduction method to solve the frequency response of large and complex FE models through automated partitioning and recursive

transformation procedure. This method has practical applications in fields of automobile engineering [30] and electromagnetics [31,32], and related studies [20–24,26,28] have been carried out. The AMLS method constructs a reduced model using the transformation matrix defined by only dominant substructural modes, the contribution of residual substructural modes is not taken into account. Since the goal of the model reduction method is to reduce the computation time with minimal loss of accuracy, the enhanced AMLS (EAMLS) method was developed [26]. The EAMLS improves the accuracy of the AMLS method considering the effect of the residual substructural modes.

The EAMLS method has created a reduced model with extremely well in terms of accuracy. However, the compensation of residual substructural modes effect for the mass and stiffness matrix, the core of EAMLS method, requires tremendous computer memory and huge computation time because it performs the Rayleigh-Ritz procedure including global matrix operation. For this reason, EAMLS method has limitations in reducing large FE models involving hundreds of thousands of DOFs. As DOFs of the FE models continues to increase, this limitations need to be resolved.

In this thesis, a new formulation of EAMLS method is presented for efficiently resolving the aforementioned limitations as follows. First, insignificant terms which are higher order terms and higher level substructure flexibility matrices are neglected. In order to reduce the large size of the substructure subspace inevitably increased, an extended root substructure is defined by assemblage of higher level substructures. Then, projection on a new refined subspace by derived the extended root substructure is employed. In the new formulation, the reduced mass and stiffness matrices are computed by submatrix (component) level instead of global matrix, and residual substructural modes correction applied only to the reduced mass matrix.

1.3 Outline

The following summarizes the thesis organization. In chapter 2, the model reduction methods related to proposed method is reviewed, including static/dynamic condensation, mode superposition method, and CMS are reviewed. In chapter 3, the AMLS and EAMLS transformation process are explained using a rectangular plate problem. To introduce the multilevel substructuring method, CMS on single level substructuring is described on multilevel context. Then, substructuring a FE model is discussed in preparation for the CMS on multilevel substructuring method. Finally, the reduced models by the AMLS and EAMLS method are defined. In chapter 4, the new formulation of EAMLS method is presented at the submatrix level. The computation bottlenecks of the EAMLS are investigated and resolved. In chapter 5, the performance of proposed method is described in comparison with AMLS and previous EAMLS methods through various numerical examples. In chapter 6, the conclusion summarizes key points of this thesis and discusses future work.

Chapter 2. Model reduction method

The finite element method (FEM) has been huge improved due to tremendous growth in computer technology, but the engineering problems beyond modern computer capacity still exist and lead to extremely time-consuming calculation. In order to transform a global model to reduced model for efficient computations with minimal loss of accuracy, model reduction method has emerged and proposed until recently [2-36]. This chapter provides briefly introduction to the condensation method, mode superposition, and component mode synthesis (CMS). See the references [1,2,4,12] for detailed descriptions of these methods.

2.1 Condensation method

In 1960s, Guyan [2] and Iron [3] first developed the condensation method that condenses minor degrees of freedom (DOFs) to major DOFs and simply ignores the inertia effect. The static condensation has an exact result for the static analysis, and this method is usually called Guyan reduction method. However, the accuracy of the reduced model is generally less accurate for the dynamic analysis due to simply neglecting the inertia effect. To alleviate this disadvantage, various extended methods called dynamic condensation method [4–10,33] have been proposed in consideration of inertia effect.

2.1.1 Static condensation

The dynamic equilibrium equations without damping can be expressed by

$$\mathbf{M}_g\ddot{\mathbf{u}}_g + \mathbf{K}_g\mathbf{u}_g = \mathbf{f}_g\,, \tag{2.1}$$

where $\mathbf{M}_g$ and $\mathbf{K}_g$ are the mass and the stiffness matrices of the global model, respectively, and $\mathbf{u}_g$ and $\mathbf{f}_g$ are the displacement response vector and external force vector for the global model, respectively. The subscript g denotes non-reduced global model quantities. The global DOFs can be partitioned as the *master* (retained) and *slave* (truncated) DOFs. The master and slave DOFs are simply indicate m and s, respectively (see Figure 2.1). Then Equation (2.1) can be partitioned as

$$\begin{bmatrix}\mathbf{M}_{m,m} & \mathbf{M}_{m,s}\\ \mathbf{M}_{s,m} & \mathbf{M}_{s,s}\end{bmatrix}\begin{bmatrix}\ddot{\mathbf{u}}_m\\ \ddot{\mathbf{u}}_s\end{bmatrix}+\begin{bmatrix}\mathbf{K}_{m,m} & \mathbf{K}_{m,s}\\ \mathbf{K}_{s,m} & \mathbf{K}_{s,s}\end{bmatrix}\begin{bmatrix}\mathbf{u}_m\\ \mathbf{u}_s\end{bmatrix}=\begin{bmatrix}\mathbf{f}_m\\ \mathbf{f}_s\end{bmatrix}. \tag{2.2}$$

Since the Guyan reduction method ignores dynamic effect, the static equation of equilibrium is used as follows

$$\begin{bmatrix}\mathbf{K}_{m,m} & \mathbf{K}_{m,s}\\ \mathbf{K}_{s,m} & \mathbf{K}_{s,s}\end{bmatrix}\begin{bmatrix}\mathbf{u}_m\\ \mathbf{u}_s\end{bmatrix}=\begin{bmatrix}\mathbf{f}_m\\ \mathbf{f}_s\end{bmatrix}. \tag{2.3}$$

Assuming that the slave external force $\mathbf{f}_s$ is to be zeros and expanding of matrix on the left-hand side of Equation (2.3), the slave displacement vector becomes

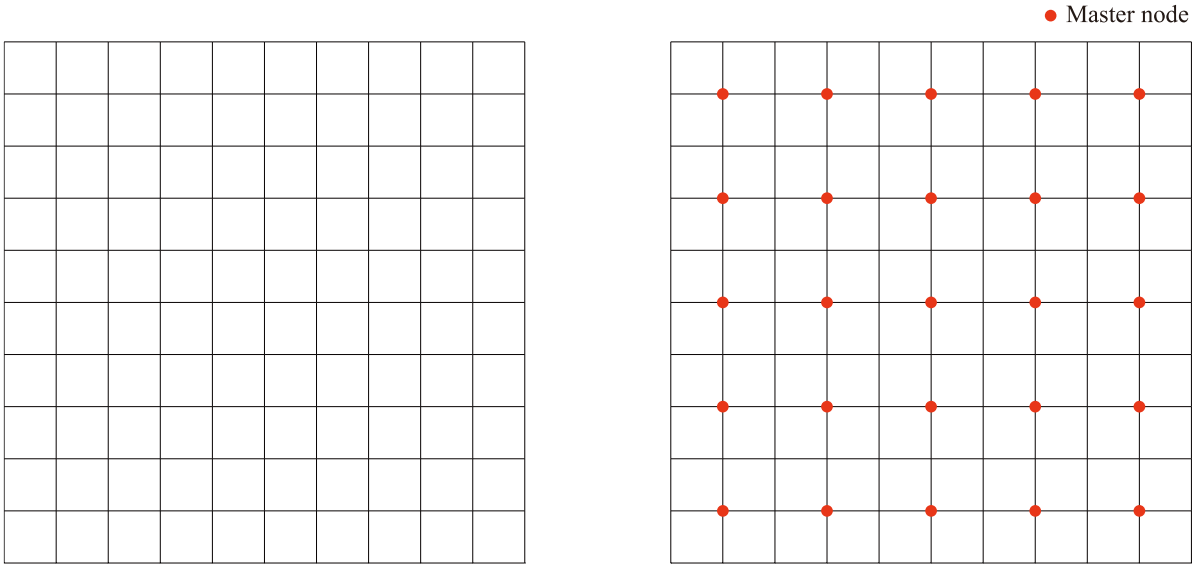

(a) (b)

Figure 2.1 DOFs selection in a rectangular plate: (a) Global model, (b) Possible DOFs selection (all nodes except for master nodes are slave nodes)

$$\mathbf{u}_s = \mathbf{\Psi}_c \mathbf{u}_m \quad \text{with} \quad \mathbf{\Psi}_c = -\mathbf{K}_{s,s}^{-1}\mathbf{K}_{s,m} \tag{2.4}$$

and then the global displacement vector is approximated as

$$\mathbf{u}_g \approx \bar{\mathbf{u}}_g = \mathbf{T}_G \mathbf{u}_m \quad \text{with} \quad \mathbf{T}_G = \begin{bmatrix} \mathbf{I}_m \\ \mathbf{\Psi}_c \end{bmatrix}, \tag{2.5}$$

in which the overbar $(\bar{\cdot})$ indicates the reduced (approximated) quantities, $\mathbf{T}_G$ is transformation matrix of Guyan reduction and $\mathbf{I}_m$ is identity matrix of same dimension as master DOFs. The subscript G indicates Guyan reduction method.

Since $\mathbf{T}_G$ is time-independent coordinate transformation matrix, $\ddot{\mathbf{u}}_g$ can be approximated by

$$\ddot{\mathbf{u}}_g \approx \ddot{\bar{\mathbf{u}}}_g = \mathbf{T}_G \ddot{\mathbf{u}}_m . \tag{2.6}$$

Substituting Equation (2.5) and (2.6) into Equation (2.1) and premultiplying the transpose of $\mathbf{T}_G$ gives

$$\begin{aligned} &\bar{\mathbf{M}}_G \ddot{\mathbf{u}}_m + \bar{\mathbf{K}}_G \mathbf{u}_m = \bar{\mathbf{f}}_G \quad \text{with} \\ &\bar{\mathbf{M}}_G = \mathbf{T}_G^T \mathbf{M}_g \mathbf{T}_G , \ \bar{\mathbf{K}}_G = \mathbf{T}_G^T \mathbf{K}_g \mathbf{T}_G , \ \bar{\mathbf{f}}_G = \mathbf{T}_G^T \mathbf{f}_g , \end{aligned} \tag{2.7}$$

where $\bar{\mathbf{M}}_G$ and $\bar{\mathbf{K}}_G$ are reduced mass and stiffness matrices in Guyan reduction, respectively, and $\bar{\mathbf{f}}_G$ is reduced force vector in Guyan reduction.

The generalized eigenvalue problem for the global model is given by

$$(\mathbf{K}_g - \lambda \mathbf{M}_g)\boldsymbol{\varphi}_g = \mathbf{0}, \tag{2.8}$$

in which λ is the eigenvalue (square of natural frequency) corresponding to global eigenvector (mode shape) $\boldsymbol{\varphi}_g$. Using the reduced mass and stiffness matrices in Equation (2.7), the reduced eigenvalue problem becomes

$$(\overline{\mathbf{K}}_G - \overline{\lambda}\overline{\mathbf{M}}_G)\boldsymbol{\varphi}_m = \mathbf{0}, \tag{2.9}$$

where $\overline{\lambda}$ is approximated eigenvalue of global model and $\boldsymbol{\varphi}_m$ is eigenvector corresponding to master DOFs. Note that static condensation has an exact solution for static problem in reduced subspace provided that $\mathbf{f}_s$ is zero.

2.1.2 Dynamic condensation

The dynamic condensation [4–10,33] is a model reduction method extending the static condensation for dynamic analysis. To achieve a more accurate solution than static condensation, the inertia effects should be partially or fully considered. This section briefly reviews the improved reduced system (IRS) method proposed O'Callahan [4] among several dynamic condensation.

Partitioning DOFs of the global FE model into master and slave DOFs as that in Section 2.1.1, the generalized eigenvalue problem for the global model in Equation (2.8) is given by

$$\left(\begin{bmatrix}\mathbf{K}_{m,m} & \mathbf{K}_{m,s}\\ \mathbf{K}_{s,m} & \mathbf{K}_{s,s}\end{bmatrix} - \lambda\begin{bmatrix}\mathbf{M}_{m,m} & \mathbf{M}_{m,s}\\ \mathbf{M}_{s,m} & \mathbf{M}_{s,s}\end{bmatrix}\right)\begin{bmatrix}\boldsymbol{\varphi}_m\\ \boldsymbol{\varphi}_s\end{bmatrix} = \begin{bmatrix}\mathbf{0}\\ \mathbf{0}\end{bmatrix}, \tag{2.10}$$

and expanding the second row on the left-hand side of Equation (2.10), $\boldsymbol{\varphi}_s$ can be expressed by

$$\boldsymbol{\varphi}_s = -(\mathbf{K}_{s,s} - \lambda\mathbf{M}_{s,s})^{-1}(\mathbf{K}_{s,m} - \lambda\mathbf{M}_{s,m})\boldsymbol{\varphi}_m. \tag{2.11}$$

Since $\boldsymbol{\varphi}_s$ given in Equation (2.11) is a nonlinear function about the unknown λ, it cannot calculated directly. Using Taylor expansion, it can be detoured and then $\boldsymbol{\varphi}_s$ is represented by

$$\boldsymbol{\varphi}_s = [-\mathbf{K}_{s,s}^{-1}\mathbf{K}_{s,m} + \lambda\mathbf{K}_{s,s}^{-1}(\mathbf{M}_{s,m} - \mathbf{M}_{s,s}\mathbf{K}_{s,s}^{-1}\mathbf{K}_{s,m}) + O(\lambda^2) + O(\lambda^3) + \cdots]\boldsymbol{\varphi}_m. \tag{2.12}$$

Neglecting the terms λ above the second order in Equation (2.12), $\boldsymbol{\varphi}_s$ is approximated as

$$\boldsymbol{\varphi}_s \approx \overline{\boldsymbol{\varphi}}_s = [-\mathbf{K}_{s,s}^{-1}\mathbf{K}_{s,m} + \lambda\mathbf{K}_{s,s}^{-1}(\mathbf{M}_{s,m} - \mathbf{M}_{s,s}\mathbf{K}_{s,s}^{-1}\mathbf{K}_{s,m})]\boldsymbol{\varphi}_m, \tag{2.13}$$

and then the global eigenvector $\boldsymbol{\varphi}_g$ can be expressed by

$$\boldsymbol{\varphi}_g \approx \overline{\boldsymbol{\varphi}}_g = \begin{bmatrix}\boldsymbol{\varphi}_m\\ \overline{\boldsymbol{\varphi}}_s\end{bmatrix} = (\mathbf{T}_G + \lambda\mathbf{T}_a)\boldsymbol{\varphi}_m \quad \text{with} \quad \mathbf{T}_a = \begin{bmatrix}\mathbf{0}\\ \mathbf{K}_{s,s}^{-1}(\mathbf{M}_{s,m} - \mathbf{M}_{s,s}\mathbf{K}_{s,s}^{-1}\mathbf{K}_{s,m})\end{bmatrix}, \tag{2.14}$$

where $\mathbf{T}_G$ is transformation matrix of Guyan reduction in Equation (2.5) and $\mathbf{T}_a$ is an additional transformation matrix considering the inertial effects of the slave DOFs.

Using Equation (2.9), the following equation is obtained

$$\overline{\lambda}\boldsymbol{\varphi}_m = \mathbf{H}_G\boldsymbol{\varphi}_m \quad \text{with} \quad \mathbf{H}_G = \overline{\mathbf{M}}_G^{-1}\overline{\mathbf{K}}_G. \tag{2.15}$$

Substituting Equation (2.15) into Equation (2.14), $\boldsymbol{\varphi}_g$ can be expressed without unknown value as

$$\boldsymbol{\varphi}_g \approx \overline{\boldsymbol{\varphi}}_g = \mathbf{T}_{IRS}\boldsymbol{\varphi}_m \quad \text{with} \quad \mathbf{T}_{IRS} = \mathbf{T}_G + \mathbf{T}_a\mathbf{H}_G\,, \tag{2.16}$$

where $\mathbf{T}_{IRS}$ is the transformation matrix of IRS method that is more accurate than the Guyan transformation matrix, and the reduced mass and stiffness matrices in the IRS method can be obtained as

$$\begin{aligned}
\overline{\mathbf{M}}_{IRS} &= \mathbf{T}_{IRS}^T\mathbf{M}_g\mathbf{T}_{IRS} = \overline{\mathbf{M}}_G + \mathbf{T}_G^T\mathbf{M}_g\mathbf{T}_a\mathbf{H}_G + \mathbf{H}_G^T\mathbf{T}_a^T\mathbf{M}_g\mathbf{T}_G + \mathbf{H}_G^T\mathbf{T}_a^T\mathbf{M}_g\mathbf{T}_a\mathbf{H}_G\,,\\
\overline{\mathbf{K}}_{IRS} &= \mathbf{T}_{IRS}^T\mathbf{K}_g\mathbf{T}_{IRS} = \overline{\mathbf{K}}_G + \mathbf{T}_G^T\mathbf{K}_g\mathbf{T}_a\mathbf{H}_G + \mathbf{H}_G^T\mathbf{T}_a^T\mathbf{K}_g\mathbf{T}_G + \mathbf{H}_G^T\mathbf{T}_a^T\mathbf{K}_g\mathbf{T}_a\mathbf{H}_G\,.
\end{aligned} \tag{2.17}$$

The IRS method is superior to Guyan reduction due to containing inertia effect. However, the reduced mass and stiffness matrices in both Guyan reduction and IRS method are highly populated, the computational cost for the solution of large system may be much expensive than the original sparse one.

2.2 Mode superposition

In the field of FEM, dynamic analysis can be performed in two groups. The first is direct integration method that solves equilibrium equations using numerical step-by-step integration. The meaning of *direct* in direct integration is that coordinate transformation is not employed. The second is mode superposition that changes the physical coordinate to generalized coordinate using global eigensolution. Although the two methods seem extraneous, in fact, they are closely related.

The computational cost of direct integration is proportional to the number of time steps and half bandwidth of system determined by the FE mesh topology and the nodal point numbering. Thus, to reduce the bandwidth, the FE mesh topology or nodal point numbering should be changed, but it is limit to obtain the minimum bandwidth in this way. On the other hand, mode superposition method can decouple the mass and stiffness matrices using orthogonality property of eigensoultion, and as a result, matrices are diagonalized.

The generalized eigenvalue problem in Equation (2.8) yields the N_g eigenpairs in which N_g is the number of DOFs in the global model. The eigenvectors are mass- and stiffness-orthogonal:

$$(\boldsymbol{\varphi}_g)_i^T\mathbf{M}_g(\boldsymbol{\varphi}_g)_j = \delta_{ij}, \quad (\boldsymbol{\varphi}_g)_i^T\mathbf{K}_g(\boldsymbol{\varphi}_g)_j = \lambda_j\delta_{ij} \quad \text{for } i \text{ and } j = 1, 2, \cdots, N_g, \tag{2.18}$$

where δ_{ij} is the Kronecker delta ($\delta_{ij} = 1$ for $i = j$, and $\delta_{ij} = 0$ for $i \neq j$).

Global displacement vector can be expressed based on eigenvector expansion theorem as

$$\mathbf{u}_g = \boldsymbol{\Phi}_g\mathbf{q}_g \quad \text{with} \quad \boldsymbol{\Phi}_g = [(\boldsymbol{\varphi}_g)_1 \quad (\boldsymbol{\varphi}_g)_2 \quad \cdots \quad (\boldsymbol{\varphi}_g)_{N_g}], \tag{2.19}$$

where $\boldsymbol{\Phi}_g$ is the time-independent global eigenvector matrix consisting of eigenvectors $\boldsymbol{\varphi}_g$, $\mathbf{q}_g$ is the generalized coordinate vector. Then, substituting Equation (2.19) into (2.1) and premultiplying by $\boldsymbol{\Phi}_g^T$, dynamic equilibrium equations become

$$\boldsymbol{\Phi}_g^T \mathbf{M}_g \boldsymbol{\Phi}_g \ddot{\mathbf{q}}_g + \boldsymbol{\Phi}^T \mathbf{K}_g \boldsymbol{\Phi}_g \mathbf{q}_g = \boldsymbol{\Phi}_g^T \mathbf{f}_g . \tag{2.20}$$

Using orthogonality properties in Equation (2.18) and (2.20) is decoupled and can be rewritten as

$$\ddot{\mathbf{q}}_g + \boldsymbol{\Lambda} \mathbf{q}_g = \boldsymbol{\Phi}_g^T \mathbf{f}_g , \tag{2.21}$$

in which $\boldsymbol{\Lambda}$ is diagonal eigenvalue matrix. The generalized displacement vector in Equation (2.21) can be numerically calculated by Duhamel integral or direct integration.

If using a full eigensolution, the solution is mathematically exact by eigenvector expansion theorem. In practice, only a few modes are retained in the eigensolution provided by a shift invert Lanczos algorithm, which reduces both the dimension of system. This method is usually called mode displacement method. The computational bottleneck of the mode superposition is that the eigenvalue problem of the large system must be solved.

2.3 Component mode synthesis

The CMS, originally proposed by Hurty [11], has been widely used to resolve the computational bottleneck of the mode superposition via component-wise approach like *divide-and-conquer*. The procedure of the CMS is broken down into following four major steps. First, the global structure is divided into several substructures (components) composed of interior and interface boundary DOFs. Next, the generalized coordinates corresponding to dominant substructural modes are defined by eigenvalue analysis of each substructure, and consequently dimension of each substructure is reduced in this step. After that, a reduced FE model is assembled or synthesized to form the global model. Finally, the response in reduced generalized coordinate transform into response in physical coordinate. The advantages of the CMS is that computational cost and required computer memory can be tremendously reduced by virtue of the analysis of smaller substructures, instead of the much larger global structure.

In accordance with the interface handling, CMS can be classified in three groups: fixed interface method [11,12,15–17], free interface method [13,18,19], and hybrid method [34]. Because the free and hybrid interface method are beyond the scope of this thesis, only the Craig-Bampton (CB) method which is a representative of fixed interface based CMS will be discussed. The CB method is still the most popular method and many extended studies [19,25,27,35,36].

For convenience to present this section, a rectangular plate model as shown in Figure 2.2(a) is taken with two substructures Ω_1, Ω_2 that share the interface boundary Γ as shown in Figure 2.2(b). The dynamic equation of motion of substructure Ω_1 can be written as

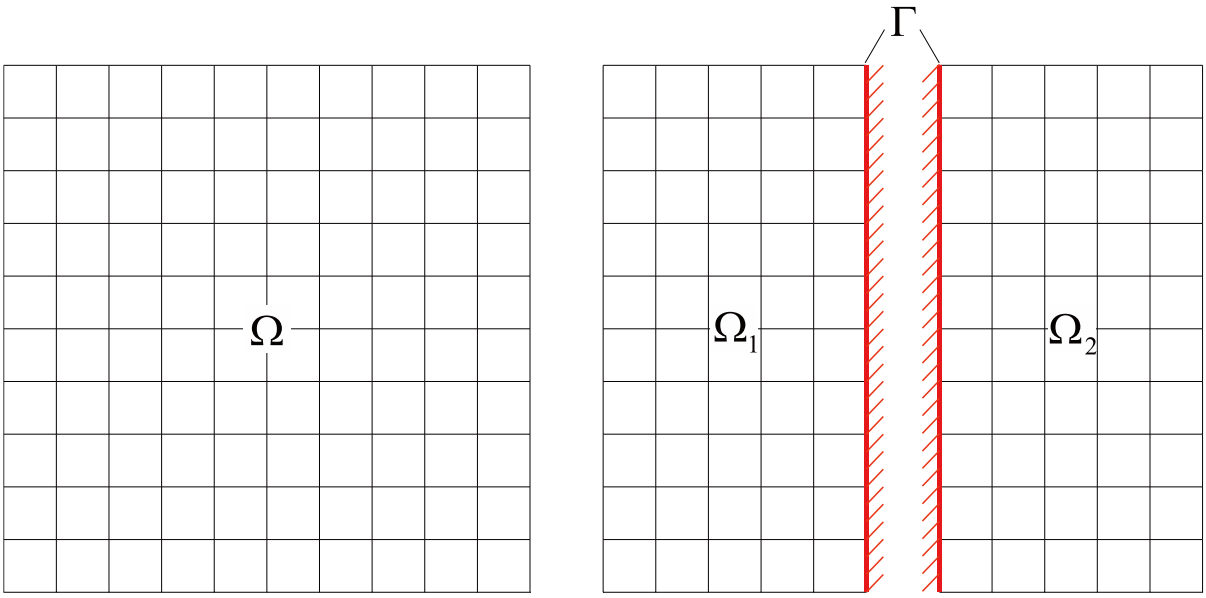

Figure 2.2 A rectangular plate with two components: (a) Global FE model, (b) Possible division of global model into two substructures with interface boundary

$$\mathbf{M}^{(1)}\ddot{\mathbf{u}}^{(1)}+\mathbf{K}^{(1)}\mathbf{u}^{(1)}=\mathbf{f}^{(1)} \quad \text{with}$$

$$\mathbf{M}^{(1)}=\begin{bmatrix}\mathbf{M}_{i,i}^{(1)} & \mathbf{M}_{i,b}^{(1)}\\ \mathbf{M}_{b,i}^{(1)} & \mathbf{M}_{b,b}^{(1)}\end{bmatrix},\ \mathbf{K}^{(1)}=\begin{bmatrix}\mathbf{K}_{i,i}^{(1)} & \mathbf{K}_{i,b}^{(1)}\\ \mathbf{K}_{b,i}^{(1)} & \mathbf{K}_{b,b}^{(1)}\end{bmatrix},\ \ddot{\mathbf{u}}^{(1)}=\begin{bmatrix}\ddot{\mathbf{u}}_i^{(1)}\\ \ddot{\mathbf{u}}_b^{(1)}\end{bmatrix},\ \mathbf{u}^{(1)}=\begin{bmatrix}\mathbf{u}_i^{(1)}\\ \mathbf{u}_b^{(1)}\end{bmatrix},\ \mathbf{f}^{(1)}=\begin{bmatrix}\mathbf{0}\\ \mathbf{f}_b^{(1)}\end{bmatrix}, \tag{2.22}$$

where the superscript (1) denotes substructure 1, and the subscripts i and b refer to interior and interface boundary DOFs, respectively. Note that interior DOFs are not subjected to external loads, because external loads are assumed to be applied to the interface boundary DOF in the CB method.

In order to reduce the dimension of substructure 1, the displacement $\mathbf{u}_i^{(1)}$ and $\mathbf{u}_b^{(1)}$ can be expressed as

$$\begin{bmatrix}\mathbf{u}_i^{(1)}\\ \mathbf{u}_b^{(1)}\end{bmatrix}=\begin{bmatrix}\boldsymbol{\Phi}^{(1)} & \boldsymbol{\Psi}_c^{(1)}\\ \mathbf{0} & \mathbf{I}\end{bmatrix}\begin{bmatrix}\mathbf{q}^{(1)}\\ \mathbf{u}_b^{(1)}\end{bmatrix}=\mathbf{T}^{(1)}\begin{bmatrix}\mathbf{q}^{(1)}\\ \mathbf{u}_b^{(1)}\end{bmatrix}, \tag{2.23}$$

in which $\mathbf{T}^{(1)}$ is the transformation matrix consisting of fixed interface normal modes matrix $\boldsymbol{\Phi}^{(1)}$ and constraint modes matrix $\boldsymbol{\Psi}_c^{(1)}$, and $\mathbf{q}^{(1)}$ is the generalized coordinate vector corresponding to $\boldsymbol{\Phi}^{(1)}$. Note that $\mathbf{I}$ is the identity matrix. The constraint modes can be defined as

$$\boldsymbol{\Psi}_c^{(1)}=-(\mathbf{K}_{i,i}^{(1)})^{-1}\mathbf{K}_{i,b}^{(1)}, \tag{2.24}$$

where the constraint modes matrix $\boldsymbol{\Psi}_c^{(1)}$ represents static deformation of the substructures by imposing unit displacement on interface boundary and is same as $\boldsymbol{\Psi}_c$ of the Guyan reduction in Equation (2.4). The fixed interface normal modes can be calculated as follows

$$\mathbf{K}_{i,i}^{(1)}\boldsymbol{\Phi}^{(1)}=\mathbf{M}_{i,i}^{(1)}\boldsymbol{\Phi}^{(1)}\boldsymbol{\Lambda}^{(1)}, \tag{2.25}$$

in which $\boldsymbol{\Phi}^{(1)}$ is the substructural eigenvector matrix corresponding to substructural eigenvalue matrix $\boldsymbol{\Lambda}^{(1)}$.

$\boldsymbol{\Phi}^{(1)}$ can be decomposed into dominant and residual substructural modes as

$$\boldsymbol{\Phi}^{(1)} = [\boldsymbol{\Phi}_d^{(1)} \quad \boldsymbol{\Phi}_r^{(1)}], \tag{2.26}$$

where superscript *d* and *r* denote the dominant and residual quantities, respectively. Substituting Equation (2.26) into Equation (2.23) gives

$$\begin{bmatrix} \mathbf{u}_i^{(1)} \\ \mathbf{u}_b^{(1)} \end{bmatrix} = \begin{bmatrix} \boldsymbol{\Phi}_d^{(1)} & \boldsymbol{\Phi}_r^{(1)} & \boldsymbol{\Psi}_c^{(1)} \\ \mathbf{0} & \mathbf{0} & \mathbf{I} \end{bmatrix} \begin{bmatrix} \mathbf{q}_d^{(1)} \\ \mathbf{q}_r^{(1)} \\ \mathbf{u}_b^{(1)} \end{bmatrix} = \mathbf{T}^{(1)} \mathbf{q}^{(1)}, \tag{2.27}$$

in which $\mathbf{q}_d^{(1)}$ and $\mathbf{q}_r^{(1)}$ represent the generalized coordinates vector of substructure 1 corresponding to dominant and residual substructural modes, respectively. Neglecting $\boldsymbol{\Phi}_r^{(1)}$ in Equation (2.27), the displacement $\mathbf{u}^{(1)}$ can be approximated by

$$\begin{bmatrix} \mathbf{u}_i^{(1)} \\ \mathbf{u}_b^{(1)} \end{bmatrix} \approx \begin{bmatrix} \overline{\mathbf{u}}_i^{(1)} \\ \mathbf{u}_b^{(1)} \end{bmatrix} = \mathbf{T}_d^{(1)} \begin{bmatrix} \mathbf{q}_d^{(1)} \\ \mathbf{u}_b^{(1)} \end{bmatrix} \quad \text{with} \quad \mathbf{T}_d^{(1)} = \begin{bmatrix} \boldsymbol{\Phi}_d^{(1)} & \boldsymbol{\Psi}_c^{(1)} \\ \mathbf{0} & \mathbf{I} \end{bmatrix}. \tag{2.28}$$

The mass and stiffness matrices, and force vector of substructure Ω_1 are transformed as follows

$$\overline{\mathbf{M}}^{(1)} = (\mathbf{T}_d^{(1)})^T \mathbf{M}^{(1)} \mathbf{T}_d^{(1)}, \quad \overline{\mathbf{K}}^{(1)} = (\mathbf{T}_d^{(1)})^T \mathbf{K}^{(1)} \mathbf{T}_d^{(1)}, \quad \overline{\mathbf{f}}^{(1)} = (\mathbf{T}_d^{(1)})^T \mathbf{f}^{(1)}, \tag{2.29}$$

where the submatrix of the reduced mass and stiffness matrices and force vector are given by

$$\begin{aligned} \overline{\mathbf{M}}^{(1)} &= \begin{bmatrix} \mathbf{I} & (\boldsymbol{\Phi}_d^{(1)})^T (\mathbf{M}_{i,b}^{(1)} + \mathbf{M}_{i,i}^{(1)} \boldsymbol{\Psi}_c^{(1)}) \\ sym. & \mathbf{M}_{b,b}^{(1)} + (\boldsymbol{\Psi}_c^{(1)})^T \mathbf{M}_{i,b}^{(1)} + (\mathbf{M}_{i,b}^{(1)})^T \boldsymbol{\Psi}_c^{(1)} + (\boldsymbol{\Psi}_c^{(1)})^T \mathbf{M}_{i,i}^{(1)} \boldsymbol{\Psi}_c^{(1)} \end{bmatrix}, \\ \overline{\mathbf{K}}^{(1)} &= \begin{bmatrix} \boldsymbol{\Lambda}_d^{(1)} & \mathbf{0} \\ \mathbf{0} & \mathbf{K}_{b,b}^{(1)} + (\mathbf{K}_{i,b}^{(1)})^T \boldsymbol{\Psi}_c^{(1)} \end{bmatrix}, \quad \overline{\mathbf{f}}^{(1)} = \begin{bmatrix} \boldsymbol{\Psi}_c^{(1)} \mathbf{f}_b^{(1)} \\ \mathbf{f}_b^{(1)} \end{bmatrix}. \end{aligned} \tag{2.30}$$

After transformation of substructure Ω_2 in the similar fashion, reduced model are assembled as

$$\begin{aligned} \overline{\mathbf{M}} &= \begin{bmatrix} \mathbf{I} & \mathbf{0} & (\boldsymbol{\Phi}_d^{(1)})^T (\mathbf{M}_{i,b}^{(1)} + \mathbf{M}_{i,i}^{(1)} \boldsymbol{\Psi}_c^{(1)}) \\ & \mathbf{I} & (\boldsymbol{\Phi}_d^{(2)})^T (\mathbf{M}_{i,b}^{(2)} + \mathbf{M}_{i,i}^{(2)} \boldsymbol{\Psi}_c^{(2)}) \\ sym. & & \sum_{n=1}^{2} \mathbf{M}_{b,b}^{(n)} + (\boldsymbol{\Psi}_c^{(n)})^T \mathbf{M}_{i,b}^{(n)} + (\mathbf{M}_{i,b}^{(n)})^T \boldsymbol{\Psi}_c^{(n)} + (\boldsymbol{\Psi}_c^{(n)})^T \mathbf{M}_{i,i}^{(n)} \boldsymbol{\Psi}_c^{(n)} \end{bmatrix}, \\ \overline{\mathbf{K}} &= \begin{bmatrix} \boldsymbol{\Lambda}_d^{(1)} & \mathbf{0} & \mathbf{0} \\ \mathbf{0} & \boldsymbol{\Lambda}_d^{(2)} & \mathbf{0} \\ \mathbf{0} & \mathbf{0} & \sum_{n=1}^{2} \mathbf{K}_{b,b}^{(n)} + (\mathbf{K}_{i,b}^{(n)})^T \boldsymbol{\Psi}_c^{(n)} \end{bmatrix}, \quad \overline{\mathbf{f}} = \begin{bmatrix} \boldsymbol{\Psi}_c^{(1)} \mathbf{f}_b^{(1)} \\ \boldsymbol{\Psi}_c^{(2)} \mathbf{f}_b^{(2)} \\ \mathbf{f}_b^{(1)} + \mathbf{f}_b^{(2)} \end{bmatrix}. \end{aligned} \tag{2.31}$$

The approximated global displacement vector can be computed by

$$\begin{bmatrix} \mathbf{u}_i^{(1)} \\ \mathbf{u}_i^{(2)} \\ \mathbf{u}_b \end{bmatrix} \approx \begin{bmatrix} \overline{\mathbf{u}}_i^{(1)} \\ \overline{\mathbf{u}}_i^{(2)} \\ \mathbf{u}_b \end{bmatrix} = \mathbf{T}_{CB} \begin{bmatrix} \mathbf{q}_i^{(1)} \\ \mathbf{q}_i^{(2)} \\ \mathbf{u}_b \end{bmatrix} \quad \text{with} \quad \mathbf{T}_{CB} = \begin{bmatrix} \boldsymbol{\Phi}_d^{(1)} & \mathbf{0} & \boldsymbol{\Psi}_c^{(1)} \\ \mathbf{0} & \boldsymbol{\Phi}_d^{(2)} & \boldsymbol{\Psi}_c^{(2)} \\ \mathbf{0} & \mathbf{0} & \mathbf{I} \end{bmatrix}. \tag{2.32}$$

In the CB method, the reduced eigenvalue problem is given by

$$(\overline{\mathbf{K}} - \overline{\lambda}\overline{\mathbf{M}})\mathbf{x}_{CB} = \mathbf{0}, \tag{2.33}$$

where $\overline{\boldsymbol{\varphi}}$ is eigenvector of the reduced model corresponding to the approximated eigenvalue of global model $\overline{\lambda}$.

Using the transformation matrix in Equation (2.32), global eigenvectors is given by back transformation

$$\boldsymbol{\varphi}_g = \mathbf{T}_{CB}\mathbf{x}_{CB}. \tag{2.34}$$

In this section, CMS on single level substructuring is presented. CMS can be also classified depending on substructuring method, and this classification will be discussed in Chapter 3.

Chapter 3. Component mode synthesis on multilevel substructuring

Traditional component mode synthesis (CMS) is the popular and effective way to reduce finite element (FE) models. However, it is difficult to apply large FE models since relatively few substructures due to the difficulty of manual partitioning have quite large DOFs. In order to resolve this limitation, the automated multilevel substructuring (AMLS) method was proposed by Bennighof et al. [15–17]. The AMLS method which extends single level to multilevel CMS decomposes global FE model to many small substructures in a purely algebraic manner without considering the physical domain.

Section 3.1 discusses the generalization of traditional CMS using the single level substructuring in multilevel context. Since then, Section 3.2 and 3.3 review the formulations of the AMLS and enhanced AMLS (EAMLS) method, respectively. See the references [15–17,26] for detailed descriptions of these methods.

3.1 Preliminary to multilevel substructuring

For the implementation of multilevel substructuring, a substructure consists only of interior DOFs without interface boundary DOFs, and interface boundary DOFs belong to interior DOFs of other substructures. In other words, the interface boundary DOFs shared with adjacent substructures is also substructure.

In this section, a rectangular plate model is taken with five substructures as shown in Figure 3.1, but the formulation can be generalized to arbitrary partitions. Figure 3.1(a) shows a possible substructuring where the areas inside the dotted line refer to areas of substructures and Figure 3.1(b) shows a graph describing to a relationships among substructures. This graph as shown in Figure 3.1(b) is called a substructure tree diagram. Substructures 1, 2, 3, and 4 are referred to as bottom level substructure that have no substructures below them on substructure tree. Substructure 5 is called the highest level substructure that have no substructures above it on substructure tree. Substructure tree diagram will be discussed in detail in the Section 3.2.1.

After partitioning the global FE model like Figure 3.1, the global stiffness matrix and displacement vector can be expressed by

$$\mathbf{K}_g = \left[\begin{array}{cccc:c} \mathbf{K}_{1,1} & & & & \mathbf{K}_{1,5} \\ & \mathbf{K}_{2,2} & & & \mathbf{K}_{2,5} \\ & & \mathbf{K}_{3,3} & & \mathbf{K}_{3,5} \\ & & & \mathbf{K}_{4,4} & \mathbf{K}_{4,5} \\ \hdashline & & \textit{sym.} & & \mathbf{K}_{5,5} \end{array}\right], \quad \mathbf{u}_g = \left[\begin{array}{c} \mathbf{u}_1 \\ \mathbf{u}_2 \\ \mathbf{u}_3 \\ \mathbf{u}_4 \\ \hdashline \mathbf{u}_5 \end{array}\right], \tag{3.1}$$

in which diagonal entries are the stiffness matrix of the each substructure and off-diagonal entries are the stiffness matrices of the each substructure coupled with highest substructure. For the consistent mass matrix, the reordered mass matrix possesses exactly the same pattern of the stiffness matrix in Equation (3.1).

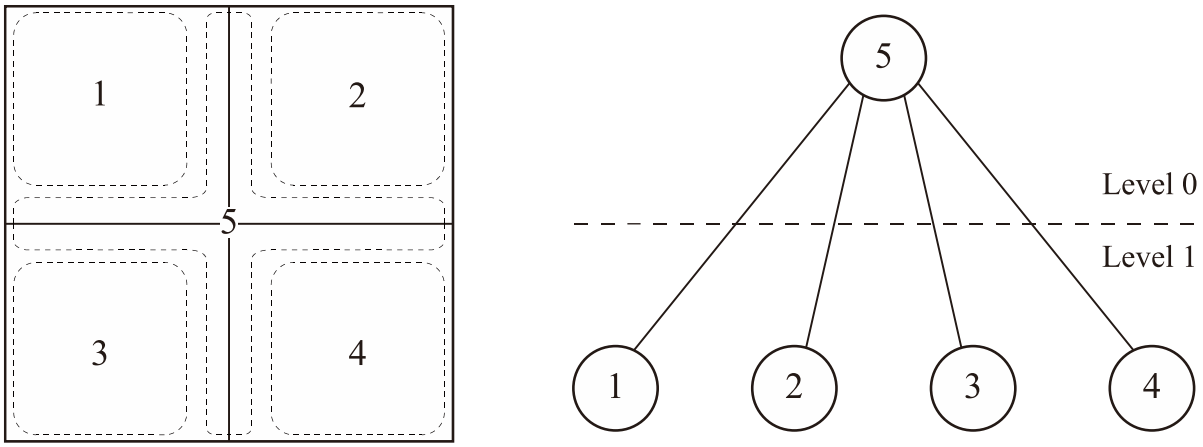

Figure 3.1 Single level substructure tree diagram for a rectangular plate: (a) Possible substructuring into five substructures, (b) Substructure tree

Starting at substructure 1, fixed interface eigenproblem of substructure 1 is

$$\mathbf{K}_{1,1}\boldsymbol{\Phi}_1 = \mathbf{M}_{1,1}\boldsymbol{\Phi}_1\boldsymbol{\Lambda}_1 \quad \text{with} \quad \boldsymbol{\Phi}_1 = [\boldsymbol{\Phi}_1^d \quad \boldsymbol{\Phi}_1^r], \quad \boldsymbol{\Lambda}_1 = \begin{bmatrix} \boldsymbol{\Lambda}_1^d & \mathbf{0} \\ \mathbf{0} & \boldsymbol{\Lambda}_1^r \end{bmatrix}, \tag{3.2}$$

in which the superscript *d* indicates eigensolution extracted lower than a given cutoff frequency value (i.e. dominant terms) and the superscript *r* indicates residual terms to be truncated according to the cutoff frequency value. Using $\boldsymbol{\Phi}_1^d$, the transformation of substructure 1 can be expressed by

$$\begin{bmatrix} \mathbf{u}_1 \\ \mathbf{u}_2 \\ \mathbf{u}_3 \\ \mathbf{u}_4 \\ \mathbf{u}_5 \end{bmatrix} = \left[\begin{array}{cccc:c} \boldsymbol{\Phi}_1^d & & & & \boldsymbol{\Psi}_{1,5} \\ & \mathbf{I}_2 & & & \\ & & \mathbf{I}_3 & & \\ & & & \mathbf{I}_4 & \\ \hdashline & & & & \mathbf{I}_5 \end{array}\right] \begin{bmatrix} \mathbf{q}_1^d \\ \mathbf{u}_2 \\ \mathbf{u}_3 \\ \mathbf{u}_4 \\ \mathbf{u}_5 \end{bmatrix} = \mathbf{T}_d^{(1)} \begin{bmatrix} \mathbf{q}_1^d \\ \mathbf{u}_2 \\ \mathbf{u}_3 \\ \mathbf{u}_4 \\ \mathbf{u}_5 \end{bmatrix} \quad \text{with} \quad \boldsymbol{\Psi}_{1,5} = -\mathbf{K}_{1,1}^{-1}\mathbf{K}_{1,5}, \tag{3.3}$$

where $\boldsymbol{\Psi}_{1,5}$ is the constraint modes matrix of substructure 1 and $\mathbf{q}_1^d$ is the generalized coordinate vector corresponding to $\boldsymbol{\Phi}_1^d$. $\mathbf{I}_i$ is the identity matrix of same dimension as the i^{th} substructure.

The transformation of substructure 2 can be also expressed by

$$\begin{bmatrix} \mathbf{q}_1^d \\ \mathbf{u}_2 \\ \mathbf{u}_3 \\ \mathbf{u}_4 \\ \mathbf{u}_5 \end{bmatrix} = \left[\begin{array}{cccc:c} \mathbf{I}_1^d & & & & \\ & \boldsymbol{\Phi}_2^d & & & \boldsymbol{\Psi}_{2,5} \\ & & \mathbf{I}_3 & & \\ & & & \mathbf{I}_4 & \\ \hdashline & & & & \mathbf{I}_5 \end{array}\right] \begin{bmatrix} \mathbf{q}_1^d \\ \mathbf{q}_2^d \\ \mathbf{u}_3 \\ \mathbf{u}_4 \\ \mathbf{u}_5 \end{bmatrix} = \mathbf{T}_d^{(2)} \begin{bmatrix} \mathbf{q}_1^d \\ \mathbf{q}_2^d \\ \mathbf{u}_3 \\ \mathbf{u}_4 \\ \mathbf{u}_5 \end{bmatrix} \quad \text{with} \quad \boldsymbol{\Psi}_{2,5} = -\mathbf{K}_{2,2}^{-1}\mathbf{K}_{2,5}, \tag{3.4}$$

in which $\mathbf{I}_1^d$ is the identity matrix with dimension equal to the number of dominant modes of substructure 1. Repeating with the transformation of substructure 3 and 4, global displacement vector can be represented by

$$\begin{bmatrix}\mathbf{u}_1\\ \mathbf{u}_2\\ \mathbf{u}_3\\ \mathbf{u}_4\\ \mathbf{u}_5\end{bmatrix} = \mathbf{T}_d \begin{bmatrix}\mathbf{q}_1^d\\ \mathbf{q}_2^d\\ \mathbf{q}_3^d\\ \mathbf{q}_4^d\\ \mathbf{u}_5\end{bmatrix} \quad \text{with} \quad \mathbf{T}_d = \mathbf{T}_d^{(1)}\mathbf{T}_d^{(2)}\mathbf{T}_d^{(3)}\mathbf{T}_d^{(4)} = \left[\begin{array}{cccc:c} \boldsymbol{\Phi}_1^d & & & & \boldsymbol{\Psi}_{1,5}\\ & \boldsymbol{\Phi}_2^d & & & \boldsymbol{\Psi}_{2,5}\\ & & \boldsymbol{\Phi}_3^d & & \boldsymbol{\Psi}_{3,5}\\ & & & \boldsymbol{\Phi}_4^d & \boldsymbol{\Psi}_{4,5}\\ \hdashline & & & & \mathbf{I}_5 \end{array}\right]. \tag{3.5}$$

Using $\mathbf{T}_d$ in Equation (3.5), reduced mass and stiffness matrices can be represented by

$\overline{\mathbf{M}} = \mathbf{T}_d^T \mathbf{M}_g \mathbf{T}_d$, $\overline{\mathbf{K}} = \mathbf{T}_d^T \mathbf{K}_g \mathbf{T}_d$ with

$$\overline{\mathbf{M}} = \begin{bmatrix} \mathbf{I}_1^d & & & & \overline{\mathbf{M}}_{1,5}\\ & \mathbf{I}_2^d & & & \overline{\mathbf{M}}_{2,5}\\ & & \mathbf{I}_3^d & & \overline{\mathbf{M}}_{3,5}\\ & \textit{sym.} & & \mathbf{I}_4^d & \overline{\mathbf{M}}_{4,5}\\ & & & & \overline{\mathbf{M}}_{5,5} \end{bmatrix}, \quad \overline{\mathbf{K}} = \begin{bmatrix} \boldsymbol{\Lambda}_1^d & & & & \\ & \boldsymbol{\Lambda}_2^d & & & \\ & & \boldsymbol{\Lambda}_3^d & & \\ & & & \boldsymbol{\Lambda}_4^d & \\ & & & & \overline{\mathbf{K}}_{5,5} \end{bmatrix} \tag{3.6}$$

where the overbar ($\bar{\cdot}$) means the approximated (reduced) quantity.

If *i* is a bottom level substructure and the *j* is the highest level substructure, the submatrices of reduced mass and stiffness matrices can be computed as

$$\mathbf{K}_{i,i}\boldsymbol{\Phi}_i = \mathbf{M}_{i,i}\boldsymbol{\Phi}_i\boldsymbol{\Lambda}_i, \tag{3.7a}$$

$$\boldsymbol{\Psi}_{i,j} = -\mathbf{K}_{i,i}^{-1}\mathbf{K}_{i,j}, \tag{3.7b}$$

$$\overline{\mathbf{K}}_{j,j}^{(i)} = \overline{\mathbf{K}}_{j,j}^{(i-1)} + \boldsymbol{\Psi}_{i,j}^T \mathbf{K}_{i,j}, \tag{3.7c}$$

$$\overline{\mathbf{M}}_{j,j}^{(i)} = \overline{\mathbf{M}}_{j,j}^{(i-1)} + \boldsymbol{\Psi}_{i,j}^T \mathbf{M}_{i,j} + \mathbf{M}_{i,j}^T \boldsymbol{\Psi}_{i,j} + \boldsymbol{\Psi}_{i,j}^T \mathbf{M}_{i,i} \boldsymbol{\Psi}_{i,j}, \tag{3.7d}$$

$$\overline{\mathbf{M}}_{i,j} = (\boldsymbol{\Phi}_i^d)^T (\mathbf{M}_{i,i}\boldsymbol{\Psi}_{i,j} + \mathbf{M}_{i,j}), \tag{3.7e}$$

where the superscript (i) denotes a matrix updated by the transformation of i^{th} substructure. In case that superscript is zero, then $(\overline{\mathbf{K}}_{j,j}^{(0)}, \overline{\mathbf{M}}_{j,j}^{(0)})$ is equal to $(\mathbf{K}_{j,j}, \mathbf{M}_{j,j})$. Note that the order of transformation of substructure has no requirement in single level substructuring method.

3.2 Automated multilevel substructuring (AMLS) method

In this section, the formulation of AMLS method is presented in the following two procedures: automated substructuring and model transformation. For convenience, a rectangular plate model is taken with two-level binary partition of seven substructures (N_s=7) in Figure 3.2.

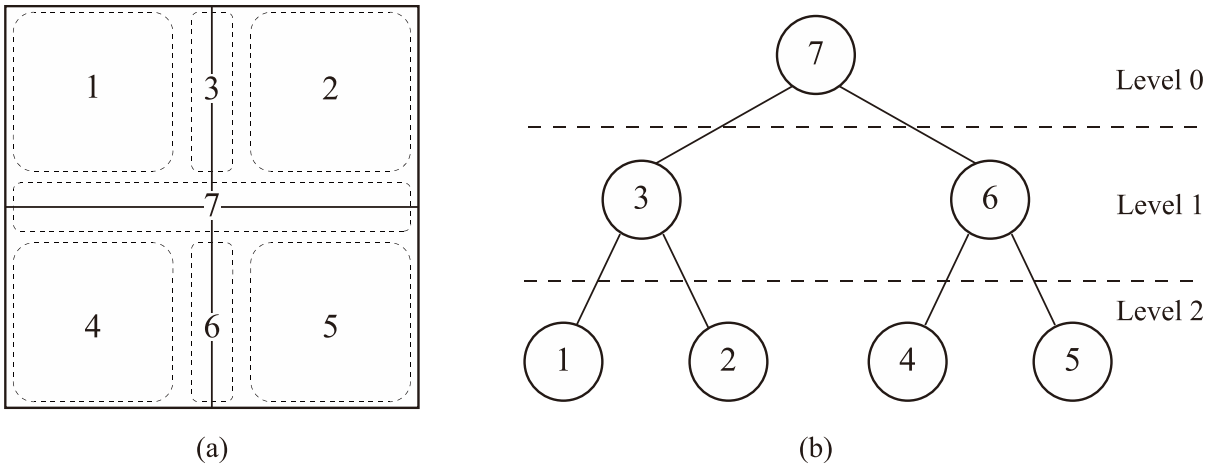

Figure 3.2 Multilevel substructure tree diagram for a rectangular plate: (a) Possible substructuring into seven substructures, (b) Substructure tree

3.2.1 Automated substructuring

For substructuring performed with manual partitioning, it is difficult to divide global FE model to a number of substructures, which leads to quite large DOFs of each substructure and induces large computational cost. Hence, the necessity of automated substructuring method in a purely algebraic manner had emerged. The nested dissection, introduced by George [37], is an algorithm for solving sparse symmetric system of linear equations based on graph partitioning and is suitable for creating substructures of a global structure. The reordering and partitioning of a matrix can be accomplished by using a graph partition program such as METIS [38] which implements the nested dissection. The METIS is used to reorder a matrix for load balancing, construct fill-reducing ordering, and so on.

Figure 3.3 describes the detailed substructuring procedure for the matrix. Figure 3.3(a) and Figure 3.3(b) show the sparsity patterns of original and reordered matrix in two-level partition as shown in Figure 3.2(b), respectively. Figure 3.3(c) shows the idealization of the sparsity pattern in Figure 3.3(b) where the each block denotes the nonzero submatrix and the diagonal entries represent the each substructure. If there is no coupled entry above the diagonal entry, this column is referred to the bottom level substructure. On the other hand, if there are any coupled entries above the diagonal entry, this column is referred to the higher level substructure. In this case, blocks 1, 2, 4, 5 represent the bottom level substructures and blocks 3, 6, 7 represent the higher level substructures.

A column coupled to the right the diagonal entry is called an *ancestor* of the row, and a row coupled to the above the diagonal entry is called a *descendant* of the column. Let C_i be defined as the set of a descendant of substructure i in which the descendant refers to the substructures below it on the substructure tree. Likewise, P_i be defined as the set of an ancestor of substructure i in which the ancestor refers to the substructures above it on substructure tree. For example, P_1 and C_7 are {3, 7} and {1, 2, 3, 4, 5, 6}, respectively. If there is no ancestor of i^{th} substructure (i.e. $P_i = \emptyset$), this substructure is called the highest level substructure.

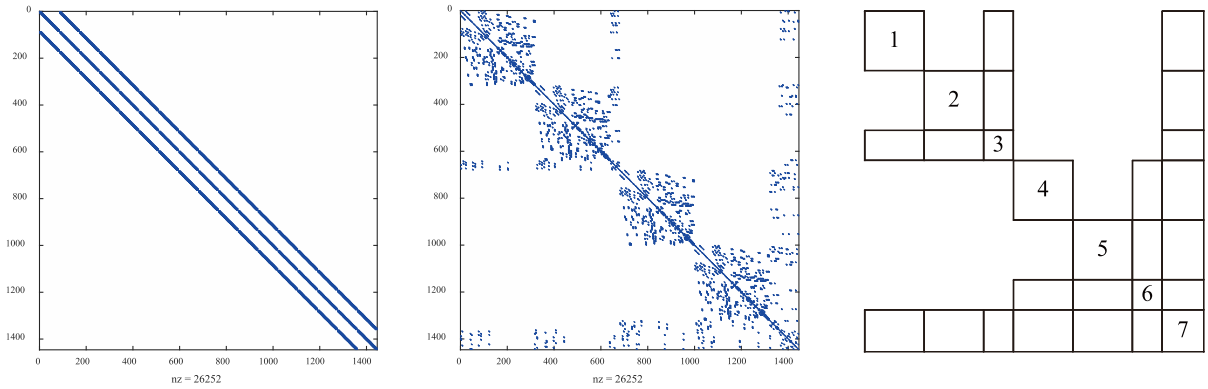

(a) (b) (c)

Figure 3.3 Sparsity patterns of matrix: (a) Original matrix, (b) Reordered matrix, (c) Idealization of sparsity pattern

In the AMLS method, two tree traversal algorithm [39] are used: preorder and postorder traversal of the tree data structure. When partitioning the matrix using the METIS, preorder traversal referred to visiting each tree node before its descendant is performed. On the other hand, when transforming the matrix, postorder traversal referred to visiting each tree node after its descendant is performed. For instance in Figure 3.2(b), the preorder and postorder traversal follow the sequences (7, 3, 1, 2, 6, 4, 5) and (1, 2, 3, 4, 5, 6, 7), respectively.

3.2.2 Model transformation

After the two level binary partition as shown in Figure 3.3(c), the global stiffness matrix $\mathbf{K}_g$ and global displacement vector $\mathbf{u}_g$ are represented by

$$\mathbf{K}_g = \begin{bmatrix} \mathbf{K}_{1,1} & & \mathbf{K}_{1,3} & & & & \mathbf{K}_{1,7} \\ & \mathbf{K}_{2,2} & \mathbf{K}_{2.3} & & & & \mathbf{K}_{2,7} \\ & & \mathbf{K}_{3,3} & & & & \mathbf{K}_{3,7} \\ & & & \mathbf{K}_{4,4} & & \mathbf{K}_{4,6} & \mathbf{K}_{4,7} \\ & & & & \mathbf{K}_{5,5} & \mathbf{K}_{5,6} & \mathbf{K}_{5,7} \\ & & \textit{sym.} & & & \mathbf{K}_{6,6} & \mathbf{K}_{6,7} \\ & & & & & & \mathbf{K}_{7,7} \end{bmatrix}, \quad \mathbf{u}_g = \begin{bmatrix} \mathbf{u}_1 \\ \mathbf{u}_2 \\ \mathbf{u}_3 \\ \mathbf{u}_4 \\ \mathbf{u}_5 \\ \mathbf{u}_6 \\ \mathbf{u}_7 \end{bmatrix}. \tag{3.8}$$

For the consistent mass matrix, the reordered mass matrix possesses exactly the same pattern of the stiffness matrix as Equation (3.8).

Starting at substructure 1, fixed interface eigenproblem of substructure 1 is

$$\mathbf{K}_{1,1}\mathbf{\Phi}_1 = \mathbf{M}_{1,1}\mathbf{\Phi}_1\mathbf{\Lambda}_1 \quad \text{with} \quad \mathbf{\Phi}_1 = [\mathbf{\Phi}_1^d \quad \mathbf{\Phi}_1^r], \quad \mathbf{\Lambda}_1 = \begin{bmatrix} \mathbf{\Lambda}_1^d & \mathbf{0} \\ \mathbf{0} & \mathbf{\Lambda}_1^r \end{bmatrix}, \tag{3.9}$$

in which the superscript *d* denotes dominant eigensolution extracted lower than a given cutoff frequency value and the superscript *r* denotes residual quantities that is eigensolution to be truncated according to the cutoff frequency value. Using $\mathbf{\Phi}_1^d$, transformation matrix of substructure 1 can be written by

$$\mathbf{T}_d^{(1)} = \begin{bmatrix} \boldsymbol{\Phi}_1^d & & \boldsymbol{\Psi}_{1,3} & & & & \boldsymbol{\Psi}_{1,7} \\ & \mathbf{I}_2 & & & & & \\ & & \mathbf{I}_3 & & & & \\ & & & \mathbf{I}_4 & & & \\ & & & & \mathbf{I}_5 & & \\ & & & & & \mathbf{I}_6 & \\ & & & & & & \mathbf{I}_7 \end{bmatrix} \quad \text{with} \quad \boldsymbol{\Psi}_{1,j} = -\mathbf{K}_{1,1}^{-1}\mathbf{K}_{1,j}, \quad \forall\, j \in P_1, \tag{3.10}$$

where the constraint modes matrix $\boldsymbol{\Psi}_{1,j}$ are computed by solving the linear equations, and $P_1 = \{3,7\}$.

Applying $\mathbf{T}_d^{(1)}$ to substructure 1 with the Rayleigh-Ritz procedure, the mass and stiffness matrices become

$$\overline{\mathbf{M}}^{(1)} = (\mathbf{T}_d^{(1)})^T \mathbf{M}_g \mathbf{T}_d^{(1)} = \begin{bmatrix} \mathbf{I}_1^d & & \boldsymbol{\mu}_{1,3}^{(1)} & & & & \boldsymbol{\mu}_{1,7}^{(1)} \\ & \mathbf{M}_{2,2} & \mathbf{M}_{2,3} & & & & \mathbf{M}_{2,7} \\ & & \hat{\mathbf{M}}_{3,3}^{(1)} & & & & \hat{\mathbf{M}}_{3,7}^{(1)} \\ & & & \mathbf{M}_{4,4} & & \mathbf{M}_{4,6} & \mathbf{M}_{4,7} \\ & & & & \mathbf{M}_{5,5} & \mathbf{M}_{5,6} & \mathbf{M}_{5,7} \\ & & \textit{sym.} & & & \mathbf{M}_{6,6} & \mathbf{M}_{6,7} \\ & & & & & & \hat{\mathbf{M}}_{7,7}^{(1)} \end{bmatrix},$$

$$\overline{\mathbf{K}}^{(1)} = (\mathbf{T}_d^{(1)})^T \mathbf{K}_g \mathbf{T}_d^{(1)} = \begin{bmatrix} \boldsymbol{\Lambda}_1^d & & \boldsymbol{\kappa}_{1,3}^{(1)} & & & & \boldsymbol{\kappa}_{1,7}^{(1)} \\ & \mathbf{K}_{2,2} & \mathbf{K}_{2,3} & & & & \mathbf{K}_{2,7} \\ & & \hat{\mathbf{K}}_{3,3}^{(1)} & & & & \hat{\mathbf{K}}_{3,7}^{(1)} \\ & & & \mathbf{K}_{4,4} & & \mathbf{K}_{4,6} & \mathbf{K}_{4,7} \\ & & & & \mathbf{K}_{5,5} & \mathbf{K}_{5,6} & \mathbf{K}_{5,7} \\ & & \textit{sym.} & & & \mathbf{K}_{6,6} & \mathbf{K}_{6,7} \\ & & & & & & \hat{\mathbf{K}}_{7,7}^{(1)} \end{bmatrix}, \tag{3.11}$$

Notice that only the ancestor of substructure 1 are affected and all other substructures are left untouched by this transformation. The submatrices of the mass and stiffness matrices can be computed by

$$\boldsymbol{\kappa}_{1,j}^{(1)} = \mathbf{0} \qquad \forall\, j \in P_1, \tag{3.12a}$$

$$\hat{\mathbf{K}}_{j,l}^{(1)} = \mathbf{K}_{j,l} + \boldsymbol{\Psi}_{1,j}^T \mathbf{K}_{1,l} \qquad \forall\, j,l \in P_1, \tag{3.12b}$$

$$\hat{\mathbf{M}}_{j,l}^{(1)} = \mathbf{M}_{j,l} + \boldsymbol{\Psi}_{1,j}^T \mathbf{M}_{1,l} + \mathbf{M}_{1,j}^T \boldsymbol{\Psi}_{1,l} + \boldsymbol{\Psi}_{1,j}^T \mathbf{M}_{1,1} \boldsymbol{\Psi}_{1,l} \qquad \forall\, j,l \in P_1, \tag{3.12c}$$

$$\boldsymbol{\mu}_{1,j}^{(1)} = \boldsymbol{\Phi}_1^T (\mathbf{M}_{1,1} \boldsymbol{\Psi}_{1,j} + \mathbf{M}_{1,j}) \qquad \forall\, j \in P_1. \tag{3.12d}$$

In the similar way, the transformation of substructure 2 is

$$\overline{\mathbf{M}}^{(2)} = (\mathbf{T}_d^{(2)})^T \overline{\mathbf{M}}^{(1)} \mathbf{T}_d^{(2)}, \tag{3.13}$$

$$\overline{\mathbf{K}}^{(2)} = (\mathbf{T}_d^{(2)})^T \overline{\mathbf{K}}^{(1)} \mathbf{T}_d^{(2)}.$$

After the transformation of substructure 2, substructure 3, the ancestor of substructure 1 and 2, is transformed

$$\overline{\mathbf{M}}^{(3)} = (\mathbf{T}_d^{(3)})^T \overline{\mathbf{M}}^{(2)} \mathbf{T}_d^{(3)} = \begin{bmatrix} \mathbf{I}_1^d & & \overline{\mathbf{M}}_{1,3} & & & & \boldsymbol{\mu}_{1,7}^{(3)} \\ & \mathbf{I}_2^d & \overline{\mathbf{M}}_{2,3} & & & & \boldsymbol{\mu}_{2,7}^{(3)} \\ & & \mathbf{I}_3^d & & & & \boldsymbol{\mu}_{3,7}^{(3)} \\ & & & \mathbf{M}_{4,4} & & \mathbf{M}_{4,6} & \mathbf{M}_{4,7} \\ & & & & \mathbf{M}_{5,5} & \mathbf{M}_{5,6} & \mathbf{M}_{5,7} \\ & & \textit{sym.} & & & \mathbf{M}_{6,6} & \mathbf{M}_{6,7} \\ & & & & & & \hat{\mathbf{M}}_{7,7}^{(3)} \end{bmatrix},$$

$$\overline{\mathbf{K}}^{(3)} = (\mathbf{T}_d^{(3)})^T \overline{\mathbf{K}}^{(2)} \mathbf{T}_d^{(3)} = \begin{bmatrix} \boldsymbol{\Lambda}_1^d & & & & & & \\ & \boldsymbol{\Lambda}_2^d & & & & & \\ & & \boldsymbol{\Lambda}_3^d & & & & \\ & & & \mathbf{K}_{4,4} & & \mathbf{K}_{4,6} & \mathbf{K}_{4,7} \\ & & & & \mathbf{K}_{5,5} & \mathbf{K}_{5,6} & \mathbf{K}_{5,7} \\ & & \textit{sym.} & & & \mathbf{K}_{6,6} & \mathbf{K}_{6,7} \\ & & & & & & \hat{\mathbf{K}}_{7,7}^{(3)} \end{bmatrix}. \tag{3.14}$$

where $\mathbf{T}_d^{(3)}$ is given by

$$\mathbf{T}_d^{(3)} = \begin{bmatrix} \mathbf{I}_1^d & & & & & & \\ & \mathbf{I}_2^d & & & & & \\ & & \boldsymbol{\Phi}_3^d & & & & \boldsymbol{\Psi}_{3,7} \\ & & & \mathbf{I}_4 & & & \\ & & & & \mathbf{I}_5 & & \\ & & & & & \mathbf{I}_6 & \\ & & & & & & \mathbf{I}_7 \end{bmatrix}. \tag{3.15}$$

$\boldsymbol{\Phi}_3^d$, $\boldsymbol{\Lambda}_3^d$, and $\boldsymbol{\Psi}_{3,7}$ in Equation (3.14) and (3.15) satisfy

$$\hat{\mathbf{K}}_{3,3}^{(2)} \boldsymbol{\Phi}_3 = \hat{\mathbf{M}}_{3,3}^{(2)} \boldsymbol{\Phi}_3 \boldsymbol{\Lambda}_3 \quad \text{with} \quad \boldsymbol{\Phi}_3 = [\boldsymbol{\Phi}_3^d \quad \boldsymbol{\Phi}_3^r], \quad \boldsymbol{\Lambda}_3 = \begin{bmatrix} \boldsymbol{\Lambda}_3^d & \mathbf{0} \\ \mathbf{0} & \boldsymbol{\Lambda}_3^r \end{bmatrix}, \tag{3.16}$$

and

$$\boldsymbol{\Psi}_{3,7} = -(\hat{\mathbf{K}}_{3,3}^{(2)})^{-1} \hat{\mathbf{K}}_{3,7}^{(2)}. \tag{3.17}$$

The changed submatrices of mass and stiffness matrices are given by

$$\hat{\mathbf{K}}_{7,7}^{(3)} = \hat{\mathbf{K}}_{7,7}^{(2)} + \boldsymbol{\Psi}_{3,7}^T \hat{\mathbf{K}}_{3,7}^{(2)}, \tag{3.18a}$$

$$\hat{\mathbf{M}}_{7,7}^{(3)} = \hat{\mathbf{M}}_{7,7}^{(2)} + \boldsymbol{\Psi}_{3,7}^T \hat{\mathbf{M}}_{3,7}^{(2)} + (\hat{\mathbf{M}}_{3,7}^{(2)})^T \boldsymbol{\Psi}_{3,7} + \boldsymbol{\Psi}_{3,7}^T \hat{\mathbf{M}}_{3,3}^{(2)} \boldsymbol{\Psi}_{3,7}\,, \tag{3.18b}$$

$$\boldsymbol{\mu}_{3,7}^{(3)} = (\boldsymbol{\Phi}_3^d)^T (\hat{\mathbf{M}}_{3,3}^{(2)} \boldsymbol{\Psi}_{3,7} + \hat{\mathbf{M}}_{3,7}^{(2)})\,, \tag{3.18c}$$

$$\boldsymbol{\mu}_{j,7}^{(3)} = \boldsymbol{\mu}_{j,3}^{(j)} \boldsymbol{\Psi}_{3,7} + \boldsymbol{\mu}_{j,7}^{(j)} \qquad \forall\, j \in C_7\,, \tag{3.18d}$$

$$\overline{\mathbf{M}}_{j,3} = \boldsymbol{\mu}_{j,3}^{(j)} \boldsymbol{\Phi}_3^d \qquad \forall\, j \in C_7\,. \tag{3.18e}$$

$\overline{\mathbf{M}}_{1,3}$ and $\overline{\mathbf{M}}_{2,3}$ in Equation (3.14) represent completely transformed terms and they will not changed by transformation of remainder substructures. When all substructures are transformed except for the highest level substructure, transformation matrix of substructure 7 is defined by

$$\mathbf{T}_d^{(7)} = \begin{bmatrix} \mathbf{I}_1^d & & & & & & \\ & \mathbf{I}_2^d & & & & & \\ & & \mathbf{I}_3^d & & & & \\ & & & \mathbf{I}_4^d & & & \\ & & & & \mathbf{I}_5^d & & \\ & & & & & \mathbf{I}_6^d & \\ & & & & & & \boldsymbol{\Phi}_7 \end{bmatrix}, \tag{3.19}$$

where a full eigensolution is computed for the highest level substructure in the AMLS method [16]

$$\hat{\mathbf{K}}_{7,7}^{(6)} \boldsymbol{\Phi}_3 = \hat{\mathbf{M}}_{7,7}^{(6)} \boldsymbol{\Phi}_3 \boldsymbol{\Lambda}_7 \;\text{ with }\; \boldsymbol{\Phi}_7 = \boldsymbol{\Phi}_7^d\,,\; \boldsymbol{\Lambda}_7 = \boldsymbol{\Lambda}_7^d\,, \tag{3.20}$$

Then the completely transformed (reduced) mass and stiffness matrices are represented by

$$\overline{\mathbf{M}} = (\mathbf{T}_d^{(7)})^T \overline{\mathbf{M}}^{(6)} \mathbf{T}_d^{(7)} = \begin{bmatrix} \mathbf{I}_1^d & & \overline{\mathbf{M}}_{1,3} & & & & \overline{\mathbf{M}}_{1,7} \\ & \mathbf{I}_2^d & \overline{\mathbf{M}}_{2,3} & & & & \overline{\mathbf{M}}_{2,7} \\ & & \mathbf{I}_3^d & & & & \overline{\mathbf{M}}_{3,7} \\ & & & \mathbf{I}_4^d & & \overline{\mathbf{M}}_{4,6} & \overline{\mathbf{M}}_{4,7} \\ & & & & \mathbf{I}_5^d & \overline{\mathbf{M}}_{5,6} & \overline{\mathbf{M}}_{5,7} \\ & & \textit{sym.} & & & \mathbf{I}_6^d & \overline{\mathbf{M}}_{6,7} \\ & & & & & & \mathbf{I}_7 \end{bmatrix}, \tag{3.21}$$

$$\overline{\mathbf{K}} = (\mathbf{T}_d^{(7)})^T \overline{\mathbf{K}}^{(6)} \mathbf{T}_d^{(7)} = diag\,(\boldsymbol{\Lambda}_1^d \quad \boldsymbol{\Lambda}_2^d \quad \boldsymbol{\Lambda}_3^d \quad \boldsymbol{\Lambda}_4^d \quad \boldsymbol{\Lambda}_5^d \quad \boldsymbol{\Lambda}_6^d \quad \boldsymbol{\Lambda}_7)\,,$$

in which *diag*(·) in Equation (3.21) denotes a block diagonal matrix and $\overline{\mathbf{M}}_{j,7}$ can be computed by

$$\overline{\mathbf{M}}_{j,7} = \boldsymbol{\mu}_{j,7}^{(j)} \boldsymbol{\Phi}_7 \qquad \forall\, j \in C_7\,. \tag{3.22}$$

The reduced mass and stiffness matrices can be also expressed

$$\overline{\mathbf{M}} = \mathbf{T}_d^T \mathbf{M}_g \mathbf{T}_d\,, \tag{3.23}$$

$$\overline{\mathbf{K}} = \mathbf{T}_d^T \mathbf{K}_g \mathbf{T}_d ,$$

where $\mathbf{T}_d$ is the dominant transformation matrix (i.e. transformation matrix of AMLS method). $\overline{\mathbf{M}}$ and $\overline{\mathbf{K}}$ are $\overline{N} \times \overline{N}$ matrices in which $\overline{N}$ is the number of dominant modes. $\mathbf{T}_d$ is given by

$$\mathbf{T}_d = \prod_{i=1}^{7} \mathbf{T}_d^{(i)} = \begin{bmatrix} \boldsymbol{\Phi}_1^d & & \hat{\boldsymbol{\Psi}}_{1,3}\boldsymbol{\Phi}_3^d & & & & \hat{\boldsymbol{\Psi}}_{1,7}\boldsymbol{\Phi}_7 \\ & \boldsymbol{\Phi}_2^d & \hat{\boldsymbol{\Psi}}_{2,3}\boldsymbol{\Phi}_3^d & & & & \hat{\boldsymbol{\Psi}}_{2,7}\boldsymbol{\Phi}_7 \\ & & \boldsymbol{\Phi}_3^d & & & & \hat{\boldsymbol{\Psi}}_{3,7}\boldsymbol{\Phi}_7 \\ & & & \boldsymbol{\Phi}_4^d & & \hat{\boldsymbol{\Psi}}_{4,6}\boldsymbol{\Phi}_6^d & \hat{\boldsymbol{\Psi}}_{4,7}\boldsymbol{\Phi}_7 \\ & & & & \boldsymbol{\Phi}_5^d & \hat{\boldsymbol{\Psi}}_{5,6}\boldsymbol{\Phi}_6^d & \hat{\boldsymbol{\Psi}}_{5,7}\boldsymbol{\Phi}_7 \\ & & & & & \boldsymbol{\Phi}_6^d & \hat{\boldsymbol{\Psi}}_{6,7}\boldsymbol{\Phi}_7 \\ & & & & & & \boldsymbol{\Phi}_7 \end{bmatrix}, \tag{3.24}$$

and may be shown that

$$\mathbf{T}_{i,j}^d = \begin{cases} \boldsymbol{\Phi}_j^d & \text{for } i = j \\ \hat{\boldsymbol{\Psi}}_{i,j}\boldsymbol{\Phi}_j^d & \text{for } i \in C_j \\ \mathbf{0} & \text{otherwise} \end{cases} . \tag{3.25}$$

in which $\mathbf{T}_{i,j}^d$ denotes a submatrix in the i^{th} row and j^{th} column of the $\mathbf{T}_d$. Multilevel extended constraint modes matrix, $\hat{\boldsymbol{\Psi}}$, can be expressed by

$$\hat{\boldsymbol{\Psi}}_{i,j} = \boldsymbol{\Psi}_{i,j} + \sum_{k \in \{P_i \cap C_j\}} \boldsymbol{\Psi}_{i,k} \hat{\boldsymbol{\Psi}}_{k,j} \qquad \forall i \in C_j . \tag{3.26}$$

Substituting multilevel extended constraint modes in Equation (3.26) into the dominant transformation matrix in Equation (3.25), the dominant transformation matrix is obtained

$$\mathbf{T}_{i,j}^d = \boldsymbol{\Psi}_{i,j}\mathbf{T}_{j,j}^d + \sum_{k \in \{P_i \cap C_j\}} \boldsymbol{\Psi}_{i,k}\mathbf{T}_{k,j}^d , \qquad \forall i \in C_j . \tag{3.27}$$

For efficient calculation of the transformation matrix, the order of operation begins $\mathbf{T}_{j,j}^d$ and moves above the column.

After all substructures have been transformed completely, reduced eigenvalue problem is defined by

$$\overline{\mathbf{K}}\mathbf{x}_d = \overline{\lambda}\,\overline{\mathbf{M}}\mathbf{x}_d \tag{3.28}$$

where $\overline{\lambda}$ is an approximation to a global eigenvalue λ in Equation (2.8). An approximated eigenvector can be obtained by

$$\boldsymbol{\varphi}_g \approx \overline{\boldsymbol{\varphi}} = \mathbf{T}_d \mathbf{x}_d \tag{3.29}$$

in which $\boldsymbol{\varphi}_g$ is a global eigenvector in Equation (2.8) and $\overline{\boldsymbol{\varphi}}$ is an approximated eigenvector.

3.3 Enhanced AMLS method

In the AMLS method, a reduced model is constructed using a transformation matrix defined dominant substructural modes only, which simply ignores the contribution of residual substructural modes. However, considering the effect of residuals substructural modes, the solution accuracy of the reduced model can be improved. Based on this fact, the enhanced AMLS (EAMLS) method [26] has been developed, which uses a residual flexibility matrix to compensate for the effect of the residual substructural mode. In this section, the formulation of EAMLS method is briefly reviewed by using the rectangular plate model in Figure 3.2.

The non-truncated transformation matrix $\mathbf{T}$ can be expressed in dominant and residual parts

$$\mathbf{T} = [\mathbf{T}_d \quad \mathbf{T}_r] \text{ with } \mathbf{T}_d = \hat{\boldsymbol{\Psi}}\boldsymbol{\Phi}_d,\ \mathbf{T}_r = \hat{\boldsymbol{\Psi}}\boldsymbol{\Phi}_r, \tag{3.30}$$

where $\boldsymbol{\Phi}_d$ and $\boldsymbol{\Phi}_r$ are dominant and residual eigenvector matrix, respectively, and they are defined by

$$\boldsymbol{\Phi}_d = diag\ (\boldsymbol{\Phi}_1^d \quad \boldsymbol{\Phi}_2^d \quad \boldsymbol{\Phi}_3^d \quad \boldsymbol{\Phi}_4^d \quad \boldsymbol{\Phi}_5^d \quad \boldsymbol{\Phi}_6^d \quad \boldsymbol{\Phi}_7), \tag{3.31a}$$

$$\boldsymbol{\Phi}_r = diag\ (\boldsymbol{\Phi}_1^r \quad \boldsymbol{\Phi}_2^r \quad \boldsymbol{\Phi}_3^r \quad \boldsymbol{\Phi}_4^r \quad \boldsymbol{\Phi}_5^r \quad \boldsymbol{\Phi}_6^r \quad \mathbf{0}). \tag{3.31b}$$

Applying the non-truncated transformation matrix $\mathbf{T}$ to the global FE model with the Rayleigh-Ritz procedure, the generalized eigenvalue problem in Equation (2.8) can be written as

$$\begin{bmatrix} \boldsymbol{\Lambda}_d - \lambda\mathbf{M}_d & -\lambda\mathbf{M}_{dr} \\ -\lambda\mathbf{M}_{dr}^T & \boldsymbol{\Lambda}_r - \lambda\mathbf{M}_r \end{bmatrix} \begin{bmatrix} \mathbf{x}_d \\ \mathbf{x}_r \end{bmatrix} = \begin{bmatrix} \mathbf{0} \\ \mathbf{0} \end{bmatrix}, \tag{3.32a}$$

$$\boldsymbol{\Lambda}_d = \mathbf{T}_d^T\mathbf{K}_g\mathbf{T}_d,\ \boldsymbol{\Lambda}_r = \mathbf{T}_r^T\mathbf{K}_g\mathbf{T}_r, \tag{3.32b}$$

$$\mathbf{M}_d = \mathbf{T}_d^T\mathbf{M}_g\mathbf{T}_d,\ \mathbf{M}_{dr} = \mathbf{T}_d^T\mathbf{M}_g\mathbf{T}_r,\ \mathbf{M}_r = \mathbf{T}_r^T\mathbf{M}_g\mathbf{T}_r, \tag{3.32c}$$

and the global eigenvector can be written by

$$\boldsymbol{\varphi}_g = \mathbf{T}\mathbf{x} = \begin{bmatrix} \mathbf{T}_d & \mathbf{T}_r \end{bmatrix} \begin{bmatrix} \mathbf{x}_d \\ \mathbf{x}_r \end{bmatrix}. \tag{3.33}$$

Expanding of the matrix on the left-hand side of Equation (3.32a), $\mathbf{x}_r$ can be written as

$$\mathbf{x}_r = \lambda(\boldsymbol{\Lambda}_r - \lambda\mathbf{M}_r)^{-1}\mathbf{M}_{dr}^T\mathbf{x}_d, \tag{3.34}$$

and substituting Equation (3.34) into Equation (3.33), the global eigenvector $\boldsymbol{\varphi}_g$ is rewritten as

$$\boldsymbol{\varphi}_g = [\mathbf{T}_d + \lambda\mathbf{T}_r(\boldsymbol{\Lambda}_r - \lambda\mathbf{M}_r)^{-1}\mathbf{M}_{dr}^T]\mathbf{x}_d. \tag{3.35}$$

Using $\mathbf{T}_r = \hat{\boldsymbol{\Psi}}\boldsymbol{\Phi}_r$ in Equation (3.30), the global eigenvector $\boldsymbol{\varphi}_g$ becomes

$$\boldsymbol{\varphi}_g = [\mathbf{T}_d + \lambda\hat{\boldsymbol{\Psi}}\mathbf{F}_r\hat{\boldsymbol{\Psi}}^T\mathbf{M}_g\mathbf{T}_d]\mathbf{x}_d \text{ with } \mathbf{F}_r = \boldsymbol{\Phi}_r(\boldsymbol{\Lambda}_r - \lambda\mathbf{M}_r)^{-1}\boldsymbol{\Phi}_r^T, \tag{3.36}$$

in which $\mathbf{F}_r$ is the residual flexibility of the substructures. $\mathbf{F}_r$ can be approximated by the first two terms of the

Taylor expansion:

$$\begin{aligned}\mathbf{F}_r &= \boldsymbol{\Phi}_r(\boldsymbol{\Lambda}_r - \lambda\mathbf{M}_r)^{-1}\boldsymbol{\Phi}_r^T \\ &\approx \boldsymbol{\Phi}_r(\boldsymbol{\Lambda}_r^{-1} - \lambda\boldsymbol{\Lambda}_r^{-1}\mathbf{M}_r\boldsymbol{\Lambda}_r^{-1})\boldsymbol{\Phi}_r^T = \mathbf{F}_{rs} + \lambda\mathbf{F}_{rm}\end{aligned}, \tag{3.37}$$

where $\mathbf{F}_{rs}$ is the static part and $\mathbf{F}_{rm}$ is the dynamic part of the residual flexibility $\mathbf{F}_r$. Substituting Equation (3.37) into Equation (3.36) and neglecting the second order λ, the global eigenvector $\boldsymbol{\varphi}_g$ can be approximated by

$$\boldsymbol{\varphi}_g \approx \overline{\boldsymbol{\varphi}} = \mathbf{T}_e\mathbf{x}_d \quad \text{with} \quad \mathbf{T}_e = \mathbf{T}_d + \lambda\mathbf{T}_a\,,\ \mathbf{T}_a = \hat{\boldsymbol{\Psi}}\mathbf{F}_{rs}\hat{\boldsymbol{\Psi}}^T\mathbf{M}_g\mathbf{T}_d \tag{3.38}$$

in which $\mathbf{T}_e$ is the enhanced transformation matrix and $\mathbf{T}_a$ is the additional transformation matrix containing residual substructural modes effect by means of $\mathbf{F}_{rs}$. Note that $\mathbf{F}_{rs}$ is indirectly computed without residual substructural eigenpair as

$$\begin{aligned}&\mathbf{F}_{rs} = \boldsymbol{\Phi}_r\boldsymbol{\Lambda}_r^{-1}\boldsymbol{\Phi}_r^T = diag(\mathbf{F}_1^{rs} \quad \mathbf{F}_2^{rs} \quad \mathbf{F}_3^{rs} \quad \mathbf{F}_4^{rs} \quad \mathbf{F}_5^{rs} \quad \mathbf{F}_6^{rs} \quad \mathbf{0}) \\ &\text{with} \quad \mathbf{F}_i^{rs} = (\hat{\mathbf{K}}_{i,i}^{(i-1)})^{-1} - \boldsymbol{\Phi}_i^d(\boldsymbol{\Lambda}_i^d)^{-1}(\boldsymbol{\Phi}_i^d)^T \quad \text{for } i = 1, 2, \cdots, N_s - 1,\end{aligned} \tag{3.39}$$

where $\left(\hat{\mathbf{K}}_{i,i}^{(i-1)}\right)^{-1}$ and $\boldsymbol{\Phi}_i^d\left(\boldsymbol{\Lambda}_i^d\right)^{-1}\left(\boldsymbol{\Phi}_i^d\right)^T$ are the full and dominant flexibility matrices for i^{th} substructure, respectively. The approximation through residual flexibility in Equation (3.38) is conceptually analogous to the static correction method [40].

By employing O'Callahan's approach in the framework of the improved reduced system (IRS) method [4] to handle the unknown λ in Equation (3.41), following relation is obtained from Equation (3.28)

$$\lambda\mathbf{x}_d = \mathbf{H}\mathbf{x}_d \quad \text{with} \quad \mathbf{H} = \overline{\mathbf{M}}^{-1}\overline{\mathbf{K}}\,. \tag{3.40}$$

Substituting Equation (3.40) into (3.38), the enhanced transformation matrix $\mathbf{T}_e$ is rewritten as

$$\mathbf{T}_e = \mathbf{T}_d + \mathbf{T}_a\mathbf{H} \quad \text{with} \quad \mathbf{T}_a = \hat{\boldsymbol{\Psi}}\mathbf{F}_{rs}\hat{\boldsymbol{\Psi}}^T\mathbf{M}_g\mathbf{T}_d\,,\ \mathbf{H} = \overline{\mathbf{M}}^{-1}\overline{\mathbf{K}}\,, \tag{3.41}$$

and using Equation (3.41), reduced mass and stiffness matrices in the EAMLS method are defined by

$$\begin{aligned}\overline{\mathbf{M}}_e &= \mathbf{T}_e^T\mathbf{M}_g\mathbf{T}_e = \overline{\mathbf{M}} + \mathbf{T}_d^T\mathbf{M}_g\mathbf{T}_a\mathbf{H} + \mathbf{H}^T\mathbf{T}_a^T\mathbf{M}_g\mathbf{T}_d + \mathbf{H}^T\mathbf{T}_a^T\mathbf{M}_g\mathbf{T}_a\mathbf{H}\,, \\ \overline{\mathbf{K}}_e &= \mathbf{T}_e^T\mathbf{K}_g\mathbf{T}_e = \overline{\mathbf{K}} + \mathbf{T}_d^T\mathbf{K}_g\mathbf{T}_a\mathbf{H} + \mathbf{H}^T\mathbf{T}_a^T\mathbf{K}_g\mathbf{T}_d + \mathbf{H}^T\mathbf{T}_a^T\mathbf{K}_g\mathbf{T}_a\mathbf{H}\,,\end{aligned} \tag{3.42}$$

in which $\overline{\mathbf{M}}_e$ and $\overline{\mathbf{K}}_e$ are $\overline{N} \times \overline{N}$ matrices, namely same size of reduced model in the AMLS method.

The reduced mass and stiffness matrices in the EAMLS method are more accurate than in the AMLS method by virtue of the residual substructural modes compensation, which is well expressed in Reference [26]. However, the EAMLS method has limitations to reduce large FE models containing over hundreds of thousands of DOFs since global matrix operation is required in constructing the enhanced transformation matrix and reduced matrices.

Chapter 4. New formulation of the enhanced AMLS method

The enhanced AMLS (EAMLS) compensates the residual substructural modes effect using the residual flexibility matrix, which can significantly improve the solution accuracy compared to the same size of reduced model obtained from the AMLS method. As the finite element (FE) model has many more degrees of freedom (DOFs), however, computational cost for explicitly employing the Rayleigh-Ritz procedure in the enhanced AMLS method can grow rapidly. DOFs of the FE models are getting bigger, and with this trend, an efficient and accurate model reduction method is needed to reduce large FE models with several millions of DOFs. Therefore, a new formulation of EAMLS method is presented through the following three sections: algebraic substructuring with reverse level order traversal, projection on a refined subspace, and the residual substructural modes correction. For convenience, a rectangular plate model is taken with two-level binary partition of seven substructures (N_s=7) in Figure 4.1

4.1 Algebraic substructuring with reverse level order traversal

In the present method, assigning substructure numbering uses the reverse level order traversal [39] referred to visiting every tree node before moving to nodes on a higher level as shown in Figure 4.1(b). On the other hand, transformation of the matrices is performed in postorder traversal or ascending numerical order. In case of Figure 4.1, the postorder traversal and ascending numerical order follow the sequences (1, 2, 5, 3, 4, 6, 7) and (1, 2, 3, 4, 5, 6, 7), respectively.

After the two level binary partition in Figure 4.1(b), the global stiffness matrix $\mathbf{K}_g$ and global displacement vector $\mathbf{u}_g$ is rearranged as

$$\mathbf{K}_g = \begin{bmatrix} \mathbf{K}_{1,1} & & & & \mathbf{K}_{1,5} & & \mathbf{K}_{1,7} \\ & \mathbf{K}_{2,2} & & & \mathbf{K}_{2,5} & & \mathbf{K}_{2,7} \\ & & \mathbf{K}_{3,3} & & & \mathbf{K}_{3,6} & \mathbf{K}_{3,7} \\ & & & \mathbf{K}_{4,4} & & \mathbf{K}_{4,6} & \mathbf{K}_{4,7} \\ & & & & \mathbf{K}_{5,5} & & \mathbf{K}_{5,7} \\ & & \textit{sym.} & & & \mathbf{K}_{6,6} & \mathbf{K}_{6,7} \\ & & & & & & \mathbf{K}_{7,7} \end{bmatrix}, \quad \mathbf{u}_g = \begin{bmatrix} \mathbf{u}_1 \\ \mathbf{u}_2 \\ \mathbf{u}_3 \\ \mathbf{u}_4 \\ \mathbf{u}_5 \\ \mathbf{u}_6 \\ \mathbf{u}_7 \end{bmatrix}. \tag{4.1}$$

The rearranged mass matrix possesses exactly the same pattern of the stiffness matrix as Equation (4.1) in the consistent mass matrix.

Let $\hat{\mathbf{T}}_d$ be the transformation matrix in AMLS procedure. Then, preliminary transformation on $\mathbf{M}_g$ and $\mathbf{K}_g$ for the new formulation results in

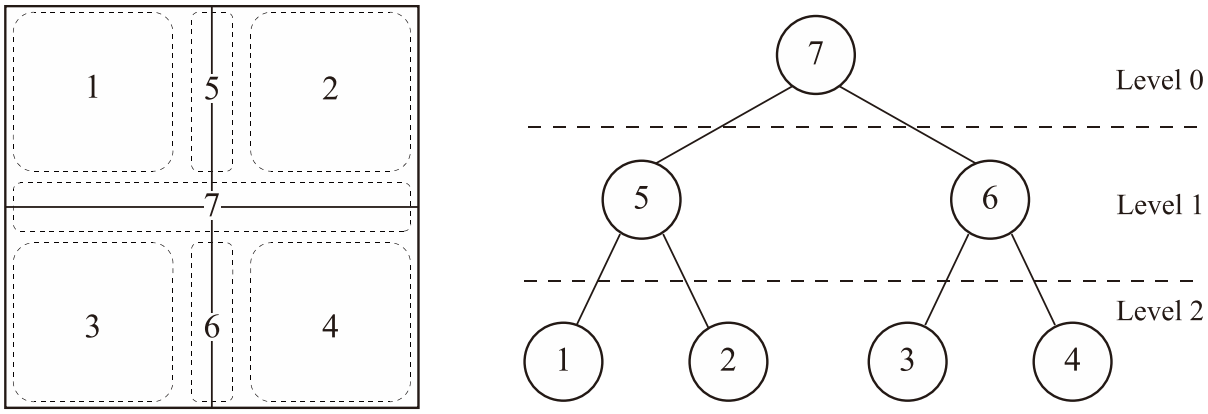

Figure 4.1 Substructure tree for the present method: (a) Possible substructuring into seven substructures (b) Substructure tree

$$\hat{\boldsymbol{\mu}} = \hat{\mathbf{T}}_d^T \mathbf{M}_g \hat{\mathbf{T}}_d = \begin{bmatrix} \mathbf{I}_1^d & & & & \hat{\boldsymbol{\mu}}_{1,5} & & \hat{\boldsymbol{\mu}}_{1,7} \\ & \mathbf{I}_2^d & & & \hat{\boldsymbol{\mu}}_{2.5} & & \hat{\boldsymbol{\mu}}_{2,7} \\ & & \mathbf{I}_3^d & & & \hat{\boldsymbol{\mu}}_{3,6} & \hat{\boldsymbol{\mu}}_{3,7} \\ & & & \mathbf{I}_4^d & & \hat{\boldsymbol{\mu}}_{4,6} & \hat{\boldsymbol{\mu}}_{4,7} \\ & & & & \mathbf{I}_5^d & & \hat{\boldsymbol{\mu}}_{5,7} \\ & & \textit{sym.} & & & \mathbf{I}_6^d & \hat{\boldsymbol{\mu}}_{6,7} \\ & & & & & & \mathbf{I}_7^d \end{bmatrix}, \tag{4.2}$$

$$\hat{\boldsymbol{\kappa}} = \hat{\mathbf{T}}_d^T \mathbf{K}_g \hat{\mathbf{T}}_d = diag(\boldsymbol{\Lambda}_1^d \quad \boldsymbol{\Lambda}_2^d \quad \boldsymbol{\Lambda}_3^d \quad \boldsymbol{\Lambda}_4^d \quad \boldsymbol{\Lambda}_5^d \quad \boldsymbol{\Lambda}_6^d \quad \boldsymbol{\Lambda}_7^d),$$

in which *diag*(·) in Equation (4.2) denotes a block diagonal matrix.

Let P_i be defined by the set of an ancestor of substructure i and C_i be defined by the set of a descendant of substructure *i*. Then, performing the recursive transformation with postorder traversal of substructure tree, the submatrices of $\hat{\boldsymbol{\mu}}$ and $\hat{\boldsymbol{\kappa}}$ in Equation (4.2) can be computed as follows

If an i^{th} substructure is bottom level substructure:

$$\mathbf{K}_{i,i}\boldsymbol{\Phi}_i = \mathbf{M}_{i,i}\boldsymbol{\Phi}_i\boldsymbol{\Lambda}_i \quad \text{with} \quad \boldsymbol{\Phi}_i = [\boldsymbol{\Phi}_i^d \quad \boldsymbol{\Phi}_i^r], \quad \boldsymbol{\Lambda}_i = \begin{bmatrix} \boldsymbol{\Lambda}_i^d & \mathbf{0} \\ \mathbf{0} & \boldsymbol{\Lambda}_i^r \end{bmatrix}, \tag{4.3a}$$

$$\boldsymbol{\Psi}_{i,j} = -\mathbf{K}_{i,i}^{-1}\mathbf{K}_{i,j} \qquad \forall\, j \in P_i, \tag{4.3b}$$

$$\hat{\boldsymbol{\kappa}}_{j,l}^{(i)} = \hat{\boldsymbol{\kappa}}_{j,l}^{(i-1)} + \boldsymbol{\Psi}_{i,j}^T \mathbf{K}_{i,l} \qquad \forall\, j,l \in P_i, \tag{4.3c}$$

$$\mathbf{m}_{j,l}^{(i)} = \mathbf{m}_{j,l}^{(i-1)} + \boldsymbol{\Psi}_{i,j}^T \mathbf{M}_{i,l} + \mathbf{M}_{i,j}^T \boldsymbol{\Psi}_{i,l} + \boldsymbol{\Psi}_{i,j}^T \mathbf{M}_{i,i} \boldsymbol{\Psi}_{i,l} \qquad \forall\, j,l \in P_i, \tag{4.3d}$$

$$\hat{\mathbf{m}}_{i,j}^{(i)} = (\boldsymbol{\Phi}_i^d)^T (\mathbf{M}_{i,i}\boldsymbol{\Psi}_{i,j} + \mathbf{M}_{i,j}) \qquad \forall\, j \in P_i, \tag{4.3e}$$

If an i^{th} substructure is higher level substructure:

$$\hat{\mathbf{\kappa}}_{i,i}^{(i-1)}\mathbf{\Phi}_i = \mathbf{m}_{i,i}^{(i-1)}\mathbf{\Phi}_i\mathbf{\Lambda}_i \quad \text{with} \quad \mathbf{\Phi}_i = [\mathbf{\Phi}_i^d \quad \mathbf{\Phi}_i^r], \quad \mathbf{\Lambda}_i = \begin{bmatrix} \mathbf{\Lambda}_i^d & \mathbf{0} \\ \mathbf{0} & \mathbf{\Lambda}_i^r \end{bmatrix}, \tag{4.4a}$$

$$\mathbf{\Psi}_{i,j} = -(\hat{\mathbf{\kappa}}_{i,i}^{(i-1)})^{-1}\hat{\mathbf{\kappa}}_{i,j}^{(i-1)} \qquad \forall\, j \in P_i, \tag{4.4b}$$

$$\hat{\mathbf{\kappa}}_{j,l}^{(i)} = \hat{\mathbf{\kappa}}_{j,l}^{(i-1)} + \mathbf{\Psi}_{i,j}^T\hat{\mathbf{\kappa}}_{i,l}^{(i-1)} \qquad \forall\, j,l \in P_i, \tag{4.4c}$$

$$\mathbf{m}_{j,l}^{(i)} = \mathbf{m}_{j,l}^{(i-1)} + \mathbf{\Psi}_{i,j}^T\mathbf{m}_{i,l}^{(i-1)} + (\mathbf{m}_{i,j}^{(i-1)})^T\mathbf{\Psi}_{i,l} + \mathbf{\Psi}_{i,j}^T\mathbf{m}_{i,i}^{(i-1)}\mathbf{\Psi}_{i,l} \qquad \forall\, j,l \in P_i, \tag{4.4d}$$

$$\hat{\mathbf{m}}_{i,j}^{(i)} = (\mathbf{\Phi}_i^d)^T(\mathbf{m}_{i,i}^{(i-1)}\mathbf{\Psi}_{i,j} + \mathbf{m}_{i,j}^{(i-1)}) \qquad \forall\, j \in P_i, \tag{4.4e}$$

$$\hat{\mathbf{m}}_{j,l}^{(i)} = \hat{\mathbf{m}}_{j,i}^{(i-1)}\mathbf{\Psi}_{i,l} + \hat{\mathbf{m}}_{j,l}^{(i-1)} \qquad \forall\, j \in C_i,\ l \in P_i, \tag{4.4f}$$

$$\hat{\mathbf{\mu}}_{j,i} = \hat{\mathbf{m}}_{j,i}^{(i-1)}\mathbf{\Phi}_i^d \qquad \forall\, j \in C_i, \tag{4.4g}$$

in which Equation (4.3a) and (4.4a) are the substructural eigenvalue problems, and the superscript d and r indicate dominant and residual quantities. If the highest excitation frequency is ω_c, eigensolutions of each substructure are extracted lower than a given cutoff frequency:

$$\lambda_B < k_B\omega_c^2, \tag{4.5a}$$

$$\lambda_H < k_H\omega_c^2. \tag{4.5b}$$

in which λ_B and λ_H are substructural eigenvalue for bottom and higher level substructures, respectively. In the AMLS and EAMLS method, the cutoff factor k_B and k_H are equal to each other, whereas in present method, k_H typically has larger value than k_B. Extracting the more eigensolutions for higher level substructures is advantageous on constructing an accurate reduced model for the same size of the reduced model due to the residual substructural mode correction for bottom level substructures. In addition, the highest level substructure eigenvalues are truncated unlike previous methods. Hence, $\hat{\mathbf{\mu}}$ and $\hat{\mathbf{\kappa}}$ are $\overline{N} \times \overline{N}$ matrices in which $\overline{N}$ is the number of dominant modes. Using the cutoff frequency, the substructural modes can be decomposed into dominant and residual substructural modes as Equation (4.3a) and (4.4a).

4.2 Projection on a refined subspace

Even in case that the cutoff factor k_B and k_H in Equation (4.5) are equal to each other, it is likely that more eigensolutions will be retained for the higher level substructures [16]. This may intuitively explained by the fact that higher level substructures are generally defined over larger domains and therefore more likely to have lower eigensolutions than bottom level substructures. Exploiting the entire subspace of reduced higher level substructures leads to expensive computational cost. Based on this fact, a new *refined* subspace is defined by selecting the eigenvector of reduced higher level substructures without losing much accuracy.

For tree data structure, the root refers to the top of the tree which is substructure 7 in Figure 4.2(a). Let an

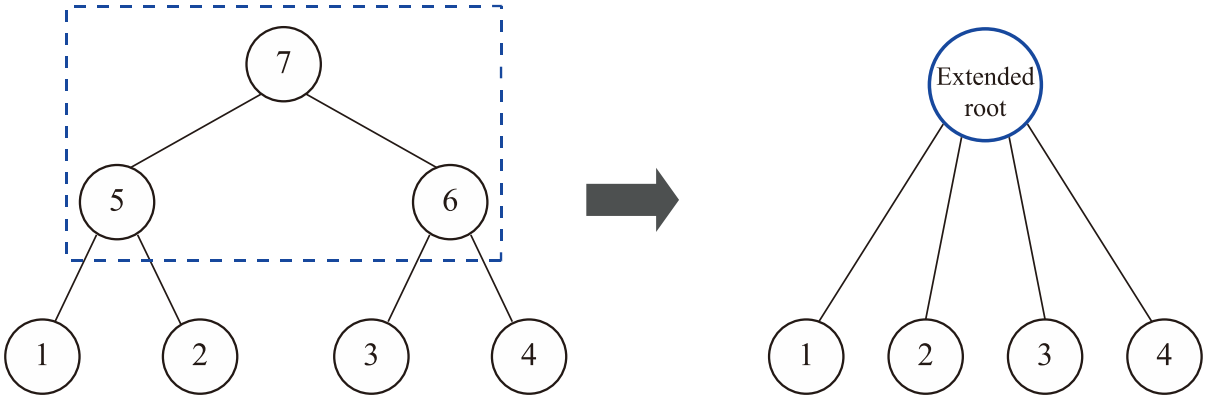

(a) (b)

Figure 4.2 Extended root assemblage process: (a) Original substructure tree (b) Substructure tree after assembling the extended root

extended root be defined by the assemblage of higher level substructures shown in Figure 4.2. Then, B is defined as a tuple of bottom level substructures, and X is defined as a tuple of extended root substructures (higher level substructures). For example in Figure 4.2, $B = (1, 2, 3, 4)$, and $X = (5, 6, 7)$.

Applying the extended root, $\hat{\boldsymbol{\mu}}$ and $\hat{\boldsymbol{\kappa}}$ can be partitioned as

$$\hat{\boldsymbol{\mu}} = \left[\begin{array}{cccc:ccc} \mathbf{I}_1^d & & & & \hat{\boldsymbol{\mu}}_{1,5} & & \hat{\boldsymbol{\mu}}_{1,7} \\ & \mathbf{I}_2^d & & & \hat{\boldsymbol{\mu}}_{2.5} & & \hat{\boldsymbol{\mu}}_{2,7} \\ & & \mathbf{I}_3^d & & & \hat{\boldsymbol{\mu}}_{3,6} & \hat{\boldsymbol{\mu}}_{3,7} \\ & & & \mathbf{I}_4^d & & \hat{\boldsymbol{\mu}}_{4,6} & \hat{\boldsymbol{\mu}}_{4,7} \\ \hdashline & & & & \mathbf{I}_5^d & & \hat{\boldsymbol{\mu}}_{5,7} \\ & & \textit{sym.} & & & \mathbf{I}_6^d & \hat{\boldsymbol{\mu}}_{6,7} \\ & & & & & & \mathbf{I}_7^d \end{array}\right], \tag{4.6}$$

$$= \left[\begin{array}{c:c} \hat{\boldsymbol{\mu}}_{B,B} & \hat{\boldsymbol{\mu}}_{B,X} \\ \hdashline \hat{\boldsymbol{\mu}}_{B,X}^T & \hat{\boldsymbol{\mu}}_{X,X} \end{array}\right]$$

$$\begin{aligned} \hat{\boldsymbol{\kappa}} &= diag(\boldsymbol{\Lambda}_1^d \quad \boldsymbol{\Lambda}_2^d \quad \boldsymbol{\Lambda}_3^d \quad \boldsymbol{\Lambda}_4^d \,\vdots\, \boldsymbol{\Lambda}_5^d \quad \boldsymbol{\Lambda}_6^d \quad \boldsymbol{\Lambda}_7^d) \\ &= diag(\hat{\boldsymbol{\kappa}}_{B,B} \,\vdots\, \hat{\boldsymbol{\kappa}}_{X,X}) \end{aligned},$$

Using the dominant and residual substructural modes in Equation (4.3a) and (4.4a), the dominant and residual substructural eigenvector matrix can be defined by

$$\begin{aligned} \hat{\boldsymbol{\Phi}}_d &= diag(\boldsymbol{\Phi}_1^d \quad \boldsymbol{\Phi}_2^d \quad \boldsymbol{\Phi}_3^d \quad \boldsymbol{\Phi}_4^d \,\vdots\, \boldsymbol{\Phi}_5^d \quad \boldsymbol{\Phi}_6^d \quad \boldsymbol{\Phi}_7^d) \\ &= diag(\boldsymbol{\Phi}_B^d \,\vdots\, \boldsymbol{\Phi}_X^d) \end{aligned}, \tag{4.7a}$$

$$\begin{aligned} \hat{\boldsymbol{\Phi}}_r &= diag(\boldsymbol{\Phi}_1^r \quad \boldsymbol{\Phi}_2^r \quad \boldsymbol{\Phi}_3^r \quad \boldsymbol{\Phi}_4^r \,\vdots\, \boldsymbol{\Phi}_5^r \quad \boldsymbol{\Phi}_6^r \quad \boldsymbol{\Phi}_7^r) \\ &= diag(\boldsymbol{\Phi}_B^r \,\vdots\, \boldsymbol{\Phi}_X^r) \end{aligned}, \tag{4.7b}$$

and dominant and residual transformation matrices are defined by

$$\hat{\mathbf{T}} = [\hat{\mathbf{T}}_d \quad \hat{\mathbf{T}}_r] \text{ with } \hat{\mathbf{T}}_d = \hat{\boldsymbol{\Psi}}\hat{\boldsymbol{\Phi}}_d,\ \hat{\mathbf{T}}_r = \hat{\boldsymbol{\Psi}}\hat{\boldsymbol{\Phi}}_r, \tag{4.8}$$

where $\hat{\mathbf{T}}_d$ can be expressed by

$$\hat{\mathbf{T}}_d = \prod_{i=1}^{6} \hat{\mathbf{T}}_d^{(i)} = \left[\begin{array}{cccc:ccc} \hat{\mathbf{T}}_{1,1}^d & & & & \hat{\mathbf{T}}_{1,5}^d & & \hat{\mathbf{T}}_{1,7}^d \\ & \hat{\mathbf{T}}_{2,2}^d & & & \hat{\mathbf{T}}_{2,5}^d & & \hat{\mathbf{T}}_{2,7}^d \\ & & \hat{\mathbf{T}}_{3,3}^d & & & \hat{\mathbf{T}}_{3,6}^d & \hat{\mathbf{T}}_{3,7}^d \\ & & & \hat{\mathbf{T}}_{4,4}^d & & \hat{\mathbf{T}}_{4,6}^d & \hat{\mathbf{T}}_{4,7}^d \\ \hdashline & & & & \hat{\mathbf{T}}_{5,5}^d & & \hat{\mathbf{T}}_{5,7}^d \\ & & & & & \hat{\mathbf{T}}_{6,6}^d & \hat{\mathbf{T}}_{6,7}^d \\ & & & & & & \hat{\mathbf{T}}_{7,7}^d \end{array}\right] = \left[\begin{array}{c:c} \hat{\mathbf{T}}_{B,B}^d & \hat{\mathbf{T}}_{B,X}^d \\ \hdashline \mathbf{0} & \hat{\mathbf{T}}_{X,X}^d \end{array}\right]. \tag{4.9}$$

where $\hat{\mathbf{T}}^{(i)}$ is the substructural transformation matrix and $\hat{\mathbf{T}}_{i,j}^d$ can be calculated at the submatrix level

$$\hat{\mathbf{T}}_{i,j}^d = \boldsymbol{\Psi}_{i,j}\hat{\mathbf{T}}_{j,j}^d + \sum_{k \in \{P_i \cap C_j\}} \boldsymbol{\Psi}_{i,k}\hat{\mathbf{T}}_{k,j}^d \qquad \forall i \in C_j. \tag{4.10}$$

The order of operation begins $\hat{\mathbf{T}}_{i,i}^d$ and moves above the column. The residual transformation matrix possesses exactly the same pattern of dominant transformation matrix as Equation (4.9). Note that the only extended root substructure matrices $\hat{\boldsymbol{\mu}}_{X,X}$ and $\hat{\boldsymbol{\kappa}}_{X,X}$ are explicitly assembled, while remainders are not assembled in this step.

After reordering the column of transformation matrix $\hat{\mathbf{T}}$ in Equation (4.8) into bottom and extended root substructures terms, the global eigenvector $\boldsymbol{\varphi}_g$ can be transformed into the projected eigenvector $\mathbf{y}$

$$\boldsymbol{\varphi}_g = \begin{bmatrix} \boldsymbol{\varphi}_B \\ \boldsymbol{\varphi}_X \end{bmatrix} = \hat{\mathbf{T}}\mathbf{y} \text{ with } \hat{\mathbf{T}} = \begin{bmatrix} \hat{\mathbf{T}}_{B,B}^d & \hat{\mathbf{T}}_{B,B}^r & \hat{\mathbf{T}}_{B,X}^d & \hat{\mathbf{T}}_{B,X}^r \\ \mathbf{0} & \mathbf{0} & \hat{\mathbf{T}}_{X,X}^d & \hat{\mathbf{T}}_{X,X}^r \end{bmatrix},\ \mathbf{y} = \begin{bmatrix} \mathbf{y}_B^d \\ \mathbf{y}_B^r \\ \mathbf{y}_X^d \\ \mathbf{y}_X^r \end{bmatrix}, \tag{4.11}$$

where the projected eigenvector $\mathbf{y}$ satisfies

$$\hat{\mathbf{K}}\mathbf{y} = \lambda\hat{\mathbf{M}}\mathbf{y} \text{ with } \hat{\mathbf{K}} = \hat{\mathbf{T}}^T\mathbf{K}_g\hat{\mathbf{T}},\ \hat{\mathbf{M}} = \hat{\mathbf{T}}^T\mathbf{M}_g\hat{\mathbf{T}}. \tag{4.12}$$

The eigenvalue problem for extended root substructure is defined by

$$\hat{\boldsymbol{\kappa}}_{X,X}\boldsymbol{\Xi} = \hat{\boldsymbol{\mu}}_{X,X}\boldsymbol{\Xi}\boldsymbol{\Theta}, \text{ with } \boldsymbol{\Xi} = [\boldsymbol{\Xi}_d \quad \boldsymbol{\Xi}_r],\ \boldsymbol{\Theta} = \begin{bmatrix} \boldsymbol{\Theta}_d & \mathbf{0} \\ \mathbf{0} & \boldsymbol{\Theta}_r \end{bmatrix} \tag{4.13}$$

where $\boldsymbol{\Xi}$ and $\boldsymbol{\Theta}$ are the eigenvector and eigenvalue matrices consisting of dominant ($\boldsymbol{\Xi}_d$ and $\boldsymbol{\Theta}_d$) and residual ($\boldsymbol{\Xi}_r$ and $\boldsymbol{\Theta}_r$) quantities for extended root substructure. The submatrices of $\boldsymbol{\Xi}_d$ can be described as

$$\boldsymbol{\Xi}_d = \begin{bmatrix} \boldsymbol{\Xi}^d_{X_1} \\ \vdots \\ \boldsymbol{\Xi}^d_{X_i} \end{bmatrix} \text{ for } i = 1, \cdots, N_H \,, \tag{4.14}$$

in which subscript X_i is the i^{th} element of tuple X, $\boldsymbol{\Xi}^d_{X_i}$ is the eigenvector of extended root substructure corresponding to X_i^{th} reduced substructure, and N_H indicates the number of higher level substructures.

Using $\boldsymbol{\Xi}$ in Equation (4.13), projected eigenvector $\mathbf{y}$ for extended root substructure can be written by

$$\begin{bmatrix} \mathbf{y}^d_X \\ \mathbf{y}^r_X \end{bmatrix} = \begin{bmatrix} \boldsymbol{\Xi}_d & \boldsymbol{\Xi}_r & \mathbf{0} \\ \mathbf{0} & \mathbf{0} & \mathbf{I} \end{bmatrix} \begin{bmatrix} \boldsymbol{\zeta}_d \\ \boldsymbol{\zeta}_r \\ \mathbf{y}^r_X \end{bmatrix}, \tag{4.15}$$

where $\boldsymbol{\zeta}_d$ and $\boldsymbol{\zeta}_r$ are denotes the generalized coordinate vectors corresponding to $\boldsymbol{\Xi}_d$ and $\boldsymbol{\Xi}_r$, respectively. Using Equation (4.15), the projected eigenvector $\mathbf{y}$ can be expressed by

$$\mathbf{y} = \begin{bmatrix} \mathbf{y}^d_B \\ \mathbf{y}^r_B \\ \mathbf{y}^d_X \\ \mathbf{y}^r_X \end{bmatrix} = \mathbf{X}\hat{\boldsymbol{\zeta}} \text{ with } \mathbf{X} = \begin{bmatrix} \mathbf{I}^d_B & \mathbf{0} & \mathbf{0} & \mathbf{0} & \mathbf{0} \\ \mathbf{0} & \mathbf{I}^r_B & \mathbf{0} & \mathbf{0} & \mathbf{0} \\ \mathbf{0} & \mathbf{0} & \boldsymbol{\Xi}_d & \boldsymbol{\Xi}_r & \mathbf{0} \\ \mathbf{0} & \mathbf{0} & \mathbf{0} & \mathbf{0} & \mathbf{I}^r_X \end{bmatrix}, \; \hat{\boldsymbol{\zeta}} = \begin{bmatrix} \mathbf{y}^d_B \\ \mathbf{y}^r_B \\ \boldsymbol{\zeta}_d \\ \boldsymbol{\zeta}_r \\ \mathbf{y}^r_R \end{bmatrix}. \tag{4.16}$$

Substituting Equation (4.16) into Equation (4.11), the global eigenvector $\boldsymbol{\varphi}_g$ is rewritten by

$$\boldsymbol{\varphi}_g = \hat{\mathbf{T}}\mathbf{y} = \tilde{\mathbf{T}}\hat{\boldsymbol{\zeta}} \text{ with } \tilde{\mathbf{T}} = \hat{\mathbf{T}}\mathbf{X} = \begin{bmatrix} \hat{\mathbf{T}}^d_{B,B} & \hat{\mathbf{T}}^r_{B,B} & \hat{\mathbf{T}}^d_{B,X}\boldsymbol{\Xi}_d & \hat{\mathbf{T}}^d_{B,X}\boldsymbol{\Xi}_r & \hat{\mathbf{T}}^r_{B,X} \\ \mathbf{0} & \mathbf{0} & \hat{\mathbf{T}}^d_{X,X}\boldsymbol{\Xi}_d & \hat{\mathbf{T}}^d_{X,X}\boldsymbol{\Xi}_r & \hat{\mathbf{T}}^r_{X,X} \end{bmatrix}. \tag{4.17}$$

After reordering the column of transformation matrix $\tilde{\mathbf{T}}$ in Equation (4.17) into dominant and residual terms, the global eigenvector $\boldsymbol{\varphi}_g$ can be transformed

$$\begin{aligned} &\boldsymbol{\varphi}_g = \tilde{\mathbf{T}}\hat{\boldsymbol{\zeta}} = [\tilde{\mathbf{T}}_d \quad \tilde{\mathbf{T}}_r] \begin{bmatrix} \hat{\boldsymbol{\zeta}}_d \\ \hat{\boldsymbol{\zeta}}_r \end{bmatrix}, \\ &\text{with } \tilde{\mathbf{T}}_d = \begin{bmatrix} \hat{\mathbf{T}}^d_{B,B} & \hat{\mathbf{T}}^d_{B,X}\boldsymbol{\Xi}_d \\ \mathbf{0} & \hat{\mathbf{T}}^d_{X,X}\boldsymbol{\Xi}_d \end{bmatrix}, \; \tilde{\mathbf{T}}_r = \begin{bmatrix} \hat{\mathbf{T}}^r_{B,B} & \hat{\mathbf{T}}^d_{B,X}\boldsymbol{\Xi}_r & \hat{\mathbf{T}}^r_{B,X} \\ \mathbf{0} & \hat{\mathbf{T}}^d_{X,X}\boldsymbol{\Xi}_r & \hat{\mathbf{T}}^r_{X,X} \end{bmatrix}, \; \hat{\boldsymbol{\zeta}}_d = \begin{bmatrix} \mathbf{y}^d_B \\ \boldsymbol{\zeta}_d \end{bmatrix}, \; \hat{\boldsymbol{\zeta}}_r = \begin{bmatrix} \mathbf{y}^r_B \\ \boldsymbol{\zeta}_r \\ \mathbf{y}^r_X \end{bmatrix}, \end{aligned} \tag{4.18}$$

and $\tilde{\mathbf{T}}_d$ and $\tilde{\mathbf{T}}_r$ may be shown that

$$\begin{aligned} &\tilde{\mathbf{T}}_d = \hat{\boldsymbol{\Psi}}\tilde{\boldsymbol{\Phi}}_d \,, \; \tilde{\mathbf{T}}_r = \hat{\boldsymbol{\Psi}}\tilde{\boldsymbol{\Phi}}_r \\ &\text{with } \tilde{\boldsymbol{\Phi}}_d = \begin{bmatrix} \boldsymbol{\Phi}^d_b & \mathbf{0} \\ \mathbf{0} & \boldsymbol{\Phi}^d_X\boldsymbol{\Xi}_d \end{bmatrix}, \; \tilde{\boldsymbol{\Phi}}_r = \begin{bmatrix} \boldsymbol{\Phi}^d_b & \mathbf{0} & \mathbf{0} \\ \mathbf{0} & \boldsymbol{\Phi}^d_X\boldsymbol{\Xi}_r & \boldsymbol{\Phi}^r_X \end{bmatrix}, \end{aligned} \tag{4.19}$$

where $\tilde{\mathbf{T}}_d$ is the refined subspace transformation matrix.

Using $\tilde{\mathbf{T}}_d$ in Equation (4.19) instead of $\hat{\mathbf{T}}_d$, mass and stiffness matrices in refined subspace are expressed

$$\tilde{\mathbf{M}} = \tilde{\mathbf{T}}_d^T \mathbf{M}_g \tilde{\mathbf{T}}_d = \begin{bmatrix} \mathbf{I}_B^d & \tilde{\mathbf{M}}_{B,X} \\ \tilde{\mathbf{M}}_{B,X}^T & \tilde{\mathbf{I}}_X^d \end{bmatrix}, \quad \tilde{\mathbf{K}} = \tilde{\mathbf{T}}_d^T \mathbf{K}_g \tilde{\mathbf{T}}_d = \begin{bmatrix} \mathbf{\Lambda}_B^d & \mathbf{0} \\ \mathbf{0} & \mathbf{\Theta}_d \end{bmatrix}, \tag{4.20}$$

in which $\tilde{\mathbf{I}}_X^d$ is the identity matrix with dimension equal to the number of column of $\mathbf{\Xi}_d$. $\tilde{\mathbf{M}}_{B,X}$ can be computed at the submatrix level as

$$\tilde{\mathbf{M}}_{B_i,X_i} = \sum_j \hat{\boldsymbol{\mu}}_{B_i,j} \mathbf{\Xi}^d_{X_j^{-1}} \quad \text{for } i = 1, \cdots, N_B, \ \forall j \in P_{B_i} \tag{4.21}$$

where the subscript B_i is i^{th} element of tuple B. X_j^{-1} is an index of j in tuple X. In other words, X_j^{-1} is defined such that $X_{X_j^{-1}} = j$. N_B indicates the number of bottom level substructures.

Applying Equation (4.20), the eigenvalue problem in refined subspace is given by

$$\tilde{\mathbf{K}}\hat{\boldsymbol{\zeta}}_d = \bar{\lambda}\tilde{\mathbf{M}}\hat{\boldsymbol{\zeta}}_d \tag{4.22}$$

4.3 Residual substructural modes correction

Using $\tilde{\mathbf{T}}$ in Equation (4.18), the eigenvalue problem in Equation (4.12) can be partitioned as

$$\begin{bmatrix} \tilde{\mathbf{\Lambda}}_d - \lambda\tilde{\mathbf{M}}_d & -\lambda\tilde{\mathbf{M}}_{dr} \\ -\lambda\tilde{\mathbf{M}}_{rd} & \tilde{\mathbf{\Lambda}}_r - \lambda\tilde{\mathbf{M}}_r \end{bmatrix} \begin{bmatrix} \hat{\boldsymbol{\zeta}}_d \\ \hat{\boldsymbol{\zeta}}_r \end{bmatrix} = \begin{bmatrix} \mathbf{0} \\ \mathbf{0} \end{bmatrix}, \tag{4.23a}$$

$$\tilde{\mathbf{\Lambda}}_d = \tilde{\mathbf{T}}_d^T \mathbf{K}_g \tilde{\mathbf{T}}_d, \ \tilde{\mathbf{\Lambda}}_r = \tilde{\mathbf{T}}_r^T \mathbf{K}_g \tilde{\mathbf{T}}_r \tag{4.23b}$$

$$\tilde{\mathbf{M}}_d = \tilde{\mathbf{T}}_d^T \mathbf{M}_g \tilde{\mathbf{T}}_d, \ \tilde{\mathbf{M}}_{dr} = \tilde{\mathbf{T}}_d^T \mathbf{M}_g \tilde{\mathbf{T}}_r, \ \tilde{\mathbf{M}}_r = \tilde{\mathbf{T}}_r^T \mathbf{M}_g \tilde{\mathbf{T}}_r. \tag{4.23c}$$

Expanding of the matrix on the left-hand side of Equation (4.23a), $\hat{\boldsymbol{\zeta}}_r$ can be written

$$\hat{\boldsymbol{\zeta}}_r = \lambda(\tilde{\mathbf{\Lambda}}_r - \lambda\tilde{\mathbf{M}}_r)^{-1}\tilde{\mathbf{M}}_{dr}^T\hat{\boldsymbol{\zeta}}_d, \tag{4.24}$$

and substituting Equation (4.24) into Equation (4.18), the global eigenvector $\boldsymbol{\varphi}_g$ is rewritten as

$$\boldsymbol{\varphi}_g = [\tilde{\mathbf{T}}_d + \lambda\tilde{\mathbf{T}}_r(\tilde{\mathbf{\Lambda}}_r - \lambda\tilde{\mathbf{M}}_r)^{-1}\tilde{\mathbf{M}}_{dr}^T]\hat{\boldsymbol{\zeta}}_d. \tag{4.25}$$

The global eigenvector $\boldsymbol{\varphi}_g$ can be expressed in dominant terms by using $\tilde{\mathbf{T}}_r = \hat{\mathbf{\Psi}}\tilde{\mathbf{\Phi}}_r$ in Equation (4.19)

$$\boldsymbol{\varphi}_g = \tilde{\mathbf{T}}_d\hat{\boldsymbol{\zeta}}_d + \lambda\hat{\mathbf{\Psi}}\tilde{\mathbf{F}}_r\hat{\mathbf{\Psi}}^T\mathbf{M}_g\hat{\mathbf{\Psi}}\tilde{\mathbf{\Phi}}_d\hat{\boldsymbol{\zeta}}_d \ \text{ with } \ \tilde{\mathbf{F}}_r = \tilde{\mathbf{\Phi}}_r(\mathbf{\Lambda}_r - \lambda\mathbf{M}_r)^{-1}\tilde{\mathbf{\Phi}}_r^T, \tag{4.26}$$

in which $\mathbf{F}_r$ is the residual flexibility of the substructures. $\mathbf{F}_r$ can be approximated by the Taylor expansion

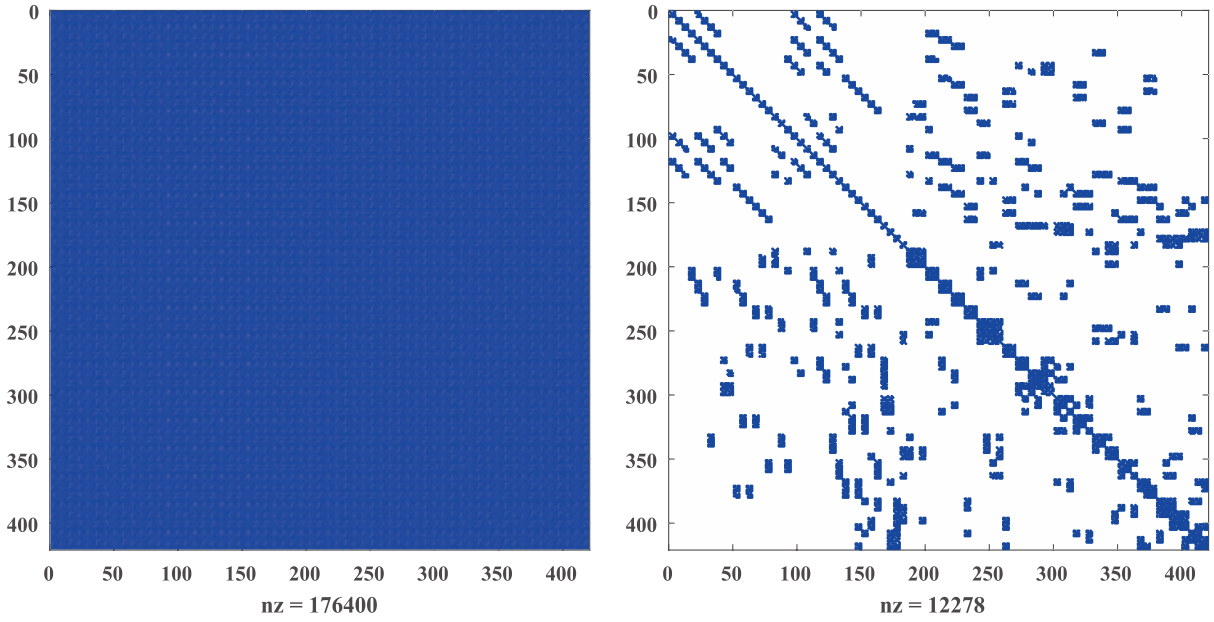

(a) (b)

Figure 4.3 Sparsity patterns for substructure: (a) Residual flexibility matrix (b) Stiffness matrix

$$\begin{aligned}\tilde{\mathbf{F}}_r &= \tilde{\mathbf{\Phi}}_r \mathbf{\Lambda}_r^{-1} \tilde{\mathbf{\Phi}}_r^T + O(\lambda) + O(\lambda^2) + \cdots \\ &\approx \tilde{\mathbf{\Phi}}_r \mathbf{\Lambda}_r^{-1} \tilde{\mathbf{\Phi}}_r^T = \hat{\mathbf{F}}_{rs}\end{aligned}, \tag{4.27}$$

where $\hat{\mathbf{F}}_{rs}$ is the static part of the residual flexibility $\mathbf{F}_r$, and can be approximated by using the only residual flexibility matrices for bottom level substructures

$$\begin{aligned}\hat{\mathbf{F}}_{rs} &\approx \begin{bmatrix} \tilde{\mathbf{F}}_B^{rs} & \mathbf{0} \\ \mathbf{0} & \mathbf{0} \end{bmatrix} \\ &= \tilde{\tilde{\mathbf{F}}}_{rs}\end{aligned} \tag{4.28}$$

with $\tilde{\mathbf{F}}_B^{rs} = diag(\tilde{\mathbf{F}}_1^{rs} \quad \cdots \quad \tilde{\mathbf{F}}_i^{rs})$, $\tilde{\mathbf{F}}_i^{rs} = \mathbf{K}_{i,i}^{-1} - \mathbf{\Phi}_i^d (\mathbf{\Lambda}_i^d)^{-1} (\mathbf{\Phi}_i^d)^T$, for $i = 1,2,\cdots N_B$.

Note that unlike the previous EAMLS method, the fully populated matrix $\mathbf{K}_{i,i}^{-1}$ in Equation (4.28) is never explicitly computed (see Figure 4.3). Instead, when used in computation, these matrices are calculated by solving the linear equations.

$\tilde{\mathbf{F}}_{rs}$ and $\bar{\lambda}$ are substituted for $\mathbf{F}_r$ and λ, respectively, the global eigenvector $\boldsymbol{\varphi}_g$ can be approximated by

$$\boldsymbol{\varphi}_g \approx (\tilde{\mathbf{T}}_d + \bar{\lambda} \tilde{\mathbf{T}}_a) \hat{\boldsymbol{\zeta}}_d$$

$$\text{with } \tilde{\mathbf{T}}_a = \hat{\mathbf{\Psi}} \tilde{\mathbf{F}}_{rs} \hat{\mathbf{\Psi}} \mathbf{M}_g \hat{\mathbf{\Psi}} \tilde{\mathbf{T}}_d = \begin{bmatrix} \tilde{\mathbf{F}}_B^{rs} \mathbf{M}_{B,B} \mathbf{\Phi}_B^d & \tilde{\mathbf{F}}_B^{rs} \mathbf{M}_{B,X} \hat{\mathbf{T}}_{X,X}^d \mathbf{\Xi}_d \\ \mathbf{0} & \mathbf{0} \end{bmatrix}. \tag{4.29}$$

Performing the Rayleigh-Ritz procedure by using Equation (4.28), the reduced mass and stiffness matrices are obtained by

$$\tilde{\mathbf{M}}_e = \tilde{\mathbf{M}} + \bar{\lambda}\tilde{\mathbf{T}}_d^T\mathbf{M}_g\tilde{\mathbf{T}}_a + \bar{\lambda}\tilde{\mathbf{T}}_a^T\mathbf{M}_g\tilde{\mathbf{T}}_d + \bar{\lambda}^2\tilde{\mathbf{T}}_a^T\mathbf{M}_g\tilde{\mathbf{T}}_a,$$
$$\tilde{\mathbf{K}}_e = \tilde{\mathbf{K}} + \bar{\lambda}\tilde{\mathbf{T}}_d^T\mathbf{K}_g\tilde{\mathbf{T}}_a + \bar{\lambda}\tilde{\mathbf{T}}_a^T\mathbf{K}_g\tilde{\mathbf{T}}_d + \bar{\lambda}^2\tilde{\mathbf{T}}_a^T\mathbf{K}_g\tilde{\mathbf{T}}_a, \tag{4.30}$$

and reduced eigenvalue problem is given by

$$[\tilde{\mathbf{K}} + \bar{\lambda}\tilde{\mathbf{T}}_d^T\mathbf{K}_g\tilde{\mathbf{T}}_a + \bar{\lambda}\tilde{\mathbf{T}}_a^T\mathbf{K}_g\tilde{\mathbf{T}}_d + \bar{\lambda}^2\tilde{\mathbf{T}}_a^T\mathbf{K}_g\tilde{\mathbf{T}}_a]\hat{\boldsymbol{\zeta}}_d$$
$$= \bar{\lambda}[\tilde{\mathbf{M}} + \bar{\lambda}\tilde{\mathbf{T}}_d^T\mathbf{M}_g\tilde{\mathbf{T}}_a + \bar{\lambda}\tilde{\mathbf{T}}_a^T\mathbf{M}_g\tilde{\mathbf{T}}_d + \bar{\lambda}^2\tilde{\mathbf{T}}_a^T\mathbf{M}_g\tilde{\mathbf{T}}_a]\hat{\boldsymbol{\zeta}}_d \tag{4.31}$$

Since $\mathbf{F}_B^{rs}$ and $\boldsymbol{\Phi}_b^d$ are orthogonal with respect to both $\mathbf{M}_{B,B}$ and $\mathbf{K}_{B,B}$, the additional transformation matrix $\tilde{\mathbf{T}}_a$ in Equation (4.29) becomes

$$\tilde{\mathbf{T}}_a = \begin{bmatrix} \mathbf{0} & \tilde{\mathbf{F}}_B^{rs}\mathbf{M}_{B,X}\hat{\mathbf{T}}_{X,X}^d\boldsymbol{\Xi}_d \\ \mathbf{0} & \mathbf{0} \end{bmatrix}. \tag{4.32}$$

Substituting Equation (4.32) into Equation (4.30), the following relations are obtained

$$\tilde{\mathbf{T}}_d^T\mathbf{M}_g\tilde{\mathbf{T}}_a = \tilde{\mathbf{T}}_a^T\mathbf{M}_g\tilde{\mathbf{T}}_d = \begin{bmatrix} \mathbf{0} & \mathbf{0} \\ \mathbf{0} & \mathbf{E}_1 \end{bmatrix} \text{ with } \mathbf{E}_1 = (\mathbf{M}_{B,X}\hat{\mathbf{T}}_{X,X}^d\boldsymbol{\Xi}_d)^T\tilde{\mathbf{F}}_B^{rs}(\mathbf{M}_{B,X}\hat{\mathbf{T}}_{X,X}^d\boldsymbol{\Xi}_d), \tag{4.33a}$$

$$\tilde{\mathbf{T}}_a^T\mathbf{M}_g\tilde{\mathbf{T}}_a = \begin{bmatrix} \mathbf{0} & \mathbf{0} \\ \mathbf{0} & \mathbf{E}_2 \end{bmatrix} \text{ with } \mathbf{E}_2 = (\mathbf{M}_{B,X}\hat{\mathbf{T}}_{X,X}^d\boldsymbol{\Xi}_d)^T\tilde{\mathbf{F}}_B^{rs}\mathbf{M}_{B,B}\tilde{\mathbf{F}}_B^{rs}(\mathbf{M}_{B,X}\hat{\mathbf{T}}_{X,X}^d\boldsymbol{\Xi}_d), \tag{4.33b}$$

$$\tilde{\mathbf{T}}_d^T\mathbf{K}_g\tilde{\mathbf{T}}_a = \tilde{\mathbf{T}}_a^T\mathbf{K}_g\tilde{\mathbf{T}}_d = \mathbf{0}, \tag{4.33c}$$

$$\tilde{\mathbf{T}}_a^T\mathbf{K}_g\tilde{\mathbf{T}}_a = \tilde{\mathbf{T}}_a^T\mathbf{M}_g\tilde{\mathbf{T}}_d, \tag{4.33d}$$

in which $\mathbf{E}_1$ can be efficiently computed at the submatrix level as

$$\mathbf{E}_1 = \sum_i \mathbf{Q}_{B_i}^T\tilde{\mathbf{F}}_{B_i}^{rs}\mathbf{Q}_{B_i}$$
$$\text{with } \mathbf{Q}_{B_i} = \sum_k\sum_j \mathbf{M}_{B_i,j}\hat{\mathbf{T}}_{j,k}^d\boldsymbol{\Xi}_{X_k^{-1}}^d \qquad \forall j \in (\{B_i\}\bigcup P_{B_i}) \text{ and } \forall k \in P_j. \tag{4.34}$$

Substituting Equation (4.33) into (4.31), the reduced eigenvalue problem in Equation (4.31) becomes

$$\tilde{\mathbf{K}}\hat{\boldsymbol{\zeta}}_d = \bar{\lambda}[\tilde{\mathbf{M}} + \bar{\lambda}\tilde{\mathbf{T}}_d^T\mathbf{M}_g\tilde{\mathbf{T}}_a + \bar{\lambda}^2\tilde{\mathbf{T}}_a^T\mathbf{M}_g\tilde{\mathbf{T}}_a]\hat{\boldsymbol{\zeta}}_d, \tag{4.35}$$

and employing O'Callahan's approach as shown in Equation (2.15) and (3.40), and neglecting the second order λ term $\bar{\lambda}^2\tilde{\mathbf{T}}_a^T\mathbf{M}_g\tilde{\mathbf{T}}_a$, a new reduced eigenproblem can be obtained

$$\tilde{\mathbf{K}}\hat{\boldsymbol{\zeta}}_d = \bar{\lambda}[\tilde{\mathbf{M}} + \tilde{\mathbf{T}}_d^T\mathbf{M}_g\tilde{\mathbf{T}}_a\tilde{\mathbf{H}}]\hat{\boldsymbol{\zeta}}_d \text{ with } \tilde{\mathbf{H}} = \tilde{\mathbf{M}}^{-1}\tilde{\mathbf{K}} = \begin{bmatrix} \tilde{\mathbf{H}}_{B,B} & \tilde{\mathbf{H}}_{B,X} \\ \tilde{\mathbf{H}}_{X,B}^* & \tilde{\mathbf{H}}_{X,X} \end{bmatrix}. \tag{4.36}$$

Notice that $\tilde{\mathbf{H}}$ in Equation (4.36) is non-symmetric matrix and therefore $\tilde{\mathbf{H}}_{X,B}^*$ does not equal to $\tilde{\mathbf{H}}_{B,X}^T$.

The submatrix for of $\hat{\zeta}_d$ can be described as

$$\hat{\zeta}_d = \begin{bmatrix} \mathbf{y}_{B_1}^d \\ \vdots \\ \mathbf{y}_{B_i}^d \\ \zeta_d \end{bmatrix} \quad \text{for} \quad i = 1, \cdots, N_B, \tag{4.37}$$

where $\mathbf{y}_{B_i}^d$ and ζ_d are the reduced eigenvector corresponding to B_i^{th} reduced substructure and extended root substructure, respectively.

Using Equation (4.33a) and (4.36), $\tilde{\mathbf{T}}_d^T \mathbf{M}_g \tilde{\mathbf{T}}_a \tilde{\mathbf{H}}$ in Equation (4.35) becomes

$$\begin{aligned} \tilde{\mathbf{T}}_d^T \mathbf{M}_g \tilde{\mathbf{T}}_a \tilde{\mathbf{H}} &= \begin{bmatrix} \mathbf{0} & \mathbf{0} \\ \mathbf{E}_1 \tilde{\mathbf{H}}_{X,B}^* & \mathbf{E}_1 \tilde{\mathbf{H}}_{X,X} \end{bmatrix} \\ &= \mathbf{C} \end{aligned} \tag{4.38}$$

in which $\mathbf{C}$ is the residual substructural modes correction matrix.

Applying Equation (4.38), the enhanced reduced mass and stiffness matrices are given

$$\begin{aligned} \tilde{\mathbf{K}}_e &= \tilde{\mathbf{K}}, \\ \tilde{\mathbf{M}}_e &= \tilde{\mathbf{M}} + \mathbf{C} \end{aligned} \tag{4.39}$$

Using $\tilde{\mathbf{H}}$ in Equation (4.36), the enhanced transformation matrix $\tilde{\mathbf{T}}_e$ is rewritten by

$$\tilde{\mathbf{T}}_e = \tilde{\mathbf{T}}_d + \tilde{\mathbf{T}}_a \tilde{\mathbf{H}}, \tag{4.40}$$

and then, global eigenvector can be obtained using back transformation procedure

$$\begin{aligned} \boldsymbol{\varphi}_g \approx \overline{\boldsymbol{\varphi}} &= \tilde{\mathbf{T}}_e \hat{\zeta}_d \\ &= \begin{bmatrix} \overline{\boldsymbol{\varphi}}_B \\ \overline{\boldsymbol{\varphi}}_X \end{bmatrix} \end{aligned} \tag{4.41}$$

in which $\overline{\boldsymbol{\varphi}}_B$ and $\overline{\boldsymbol{\varphi}}_X$ are calculated by

$$\overline{\boldsymbol{\varphi}}_{B_i} = \hat{\mathbf{T}}_{B_i,B_i}^d \mathbf{y}_{B_i}^d + \left(\sum_j \hat{\mathbf{T}}_{B_i,j}^d \boldsymbol{\Xi}_{X_j^{-1}}^d \right) \zeta_d + \left(\sum_i \tilde{\mathbf{F}}_{B_i}^{rs} \mathbf{Q}_{B_i} \right) (\tilde{\mathbf{H}}_{X,B}^* \mathbf{y}_B^d + \tilde{\mathbf{H}}_{X,X} \zeta_d) \tag{4.42a}$$

$$\overline{\boldsymbol{\varphi}}_X = \left(\sum_j \hat{\mathbf{T}}_{X,j}^d \boldsymbol{\Xi}_j^d \right) \zeta_d \tag{4.42b}$$

where $\tilde{\mathbf{F}}_B^{rs} \mathbf{Q}_B$ in Equation (4.42a) is already computed in Equation (4.34).

Table 4.1 describes the algorithm of the present EAMLS method.

Table 4.1 Algorithm of the present enhanced AMLS method

Step 1. *Algebraic substructuring with reverse level order traversal*

Step 2. *Preliminary transformation on* $\mathbf{M}_g$ *and* $\mathbf{K}_g$

<For bottom level substructures>

a. Solve the substructural eigenproblem in Equation (4.3a)

b. Calculate the constraint modes in Equation (4.3b)

c. Update the ancestors of substructure in Equation (4.3c), (4.3d), and (4.3e)

<For bottom level substructures>

a. Solve the substructural eigenproblem in Equation (4.4a)

b. Calculate the constraint modes in Equation (4.4b)

c. Update the ancestors of substructure in Equation (4.4c), (4.4d), and (4.4e)

d. Update the descendant of substructure in Equation (4.4f)

e. Calculate the completely transformed descendant of substructure in Equation (4.4g)

Step 3. *Projection on the refined subspace*

a. Assemble the extended root substructure $\hat{\boldsymbol{\mu}}_{X,X}$ and $\hat{\boldsymbol{\kappa}}_{X,X}$

b. Solve the eigenproblem for extended root substructure in Equation (4.13)

c. Projection on the refined subspace in Equation (4.20) and (4.21)

Step 4. *Residual substructural modes correction*

a. Calculate $\mathbf{E}_1$ and $\tilde{\mathbf{H}}$ in Equation (4.34) and (4.36)

b. Calculate the residual substructural modes correction matrix $\mathbf{C}$ in Equation (4.38)

c. Construct the reduced mass and stiffness matrices in Equation (4.39)

Step 5. *Reduced eigenproblem*

Solve the reduced eigenproblem in Equation (4.36)

Step 6. *Back transformation procedure*

Calculate the global eigenvector by back transformation procedure in Equation (4.42)

Chapter 5. Numerical examples

In this chapter, four numerical examples including a rectangular plate, a centrifugal impeller, a femur bone, and an airplane fuselage in free vibration condition are presented to verify the overall performance of the proposed method. The reduced model is constructed by using the AMLS, previous and present EAMLS method, respectively, and the performance are judged primarily on the accuracy of solution and elapsed time. The solution accuracy of reduced model be evaluated on the following relative eigenvalue error

$$\gamma_i = \frac{\overline{\lambda}_i - \lambda_i}{\lambda_i}, \tag{5.1}$$

where γ_i is the relative eigenvalue error, and $\overline{\lambda}_i$ and λ_i are the approximated and reference (global) eigenvalue corresponding to the i^{th} mode.

The METIS [38], unstructured graph partition program, is used for algebraic substructuring and the number of substructures is equal in the AMLS, previous and present EAMLS method. The frequency cutoff value is adopt as the criterion for selecting dominant substructural modes. All numerical computations were performed by MATLAB 2016b under Windows 10 operating system with an Intel Core i7 7700 3.60 GHz, 32 GB RAM.

5.1 Rectangular plate problem

A rectangular plate in Figure 5.1 is considered. Length L is 20 m, width B is 12 m, thickness is 0.01 m, Young's modulus E is 207 GPa, Poisson's ratio ν is 0.3, and density ρ is 7850 kg/m^3. The plate is modeled by 30×24 mesh (3875 DOFs) of the MITC4 shell element [41] and the reference eigenvalues are written in Appendix. The reduced models obtained from the AMLS, previous and present EAMLS are constructed in the same size.

In this problem, the relative eigenvalue error in Equation (5.1), modal assurance criterion (MAC), and relative eigenvector error ε_i, defined using MAC, are used to evaluate the accuracy of the methods as follows

$$\mathrm{MAC}_{i,j} = \frac{(\boldsymbol{\varphi}_i \cdot \overline{\boldsymbol{\varphi}}_j)^2}{(\boldsymbol{\varphi}_i \cdot \boldsymbol{\varphi}_i)(\overline{\boldsymbol{\varphi}}_j \cdot \overline{\boldsymbol{\varphi}}_j)}, \tag{5.2}$$

$$\varepsilon_i = \arccos(\mathrm{MAC}_{i,i}). \tag{5.3}$$

where $\overline{\boldsymbol{\varphi}}_i$ and $\boldsymbol{\varphi}_i$ are the approximated and reference (global) eigenvector corresponding to the i^{th} eigenvalue. The global structure is partitioined into 15 substructures using algebraic substructuring in AMLS, and previous and present EAMLS methods and compared two different error tolerance in the AMLS method:

- Case A: The relative eigenvalue errors in the AMLS method up to the 20^{th} mode are greater than 0.01. For AMLS and previous EAMLS methods, the number of DOFs of the reduced bottom and higher level substructures are 8 and 141, respectively. For present EAMLS methods, the number of DOFs of the reduced bottom level substurctures and extended root substructure are 60 and 89, respectively. Therefore, the number of DOFs of reduced models are 149.

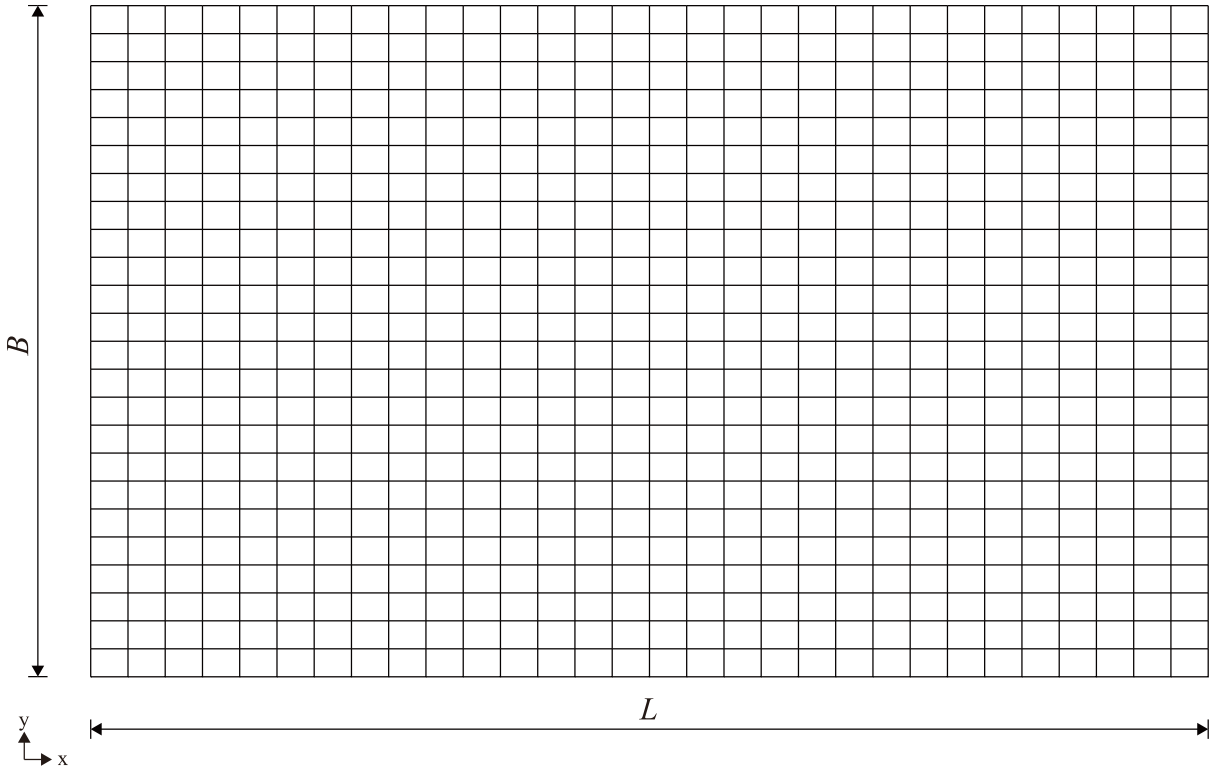

Figure 5.1 A rectangular plate model

- Case B: The relative eigenvalue errors in the AMLS method up to the 20^{th} mode are less than 0.01. For AMLS and previous EAMLS methods, the number of DFOS of the reduced bottom and higher level substructures are 46 and 163, respectively. For present EAMLS methods, the number of DOFs of the reduced bottom level substructures and extended root substructure on refined subspace are 91 and 118, respectively. Therefore, the number of DOFs of reduced models are 209.

Figure 5.2 represents the relative eigenvalue errors for each case, and Table 5.1 present the relative eigenvalue errors for Case A. Figure 5.3 and 5.4 represent the MAC values and relative eigenvector errors for Case A. The results of Case A demonstrate the improved accuracy of the present method compared to the AMLS methods, and the tiny loss in accuracy compared to the previous EAMLS method. On the other hand, in Case B, the accuracy of the present method has been improved compared to the AMLS method, while slight bigger loss in accuracy occurs compared to the previous EAMLS method than Case A. Table 5.2 and 5.3 describe the computational cost for each method. Table 5.2 show that the present method only requires 1.04 times more computational cost than the AMLS method and 3.44 times faster than previous EAMLS method. Table 5.3 show that the present method only requires 1.07 times more computational cost than the AMLS method and 3.54 times faster than previous EAMLS method. The efficiency of present method is guaranteed in both cases.

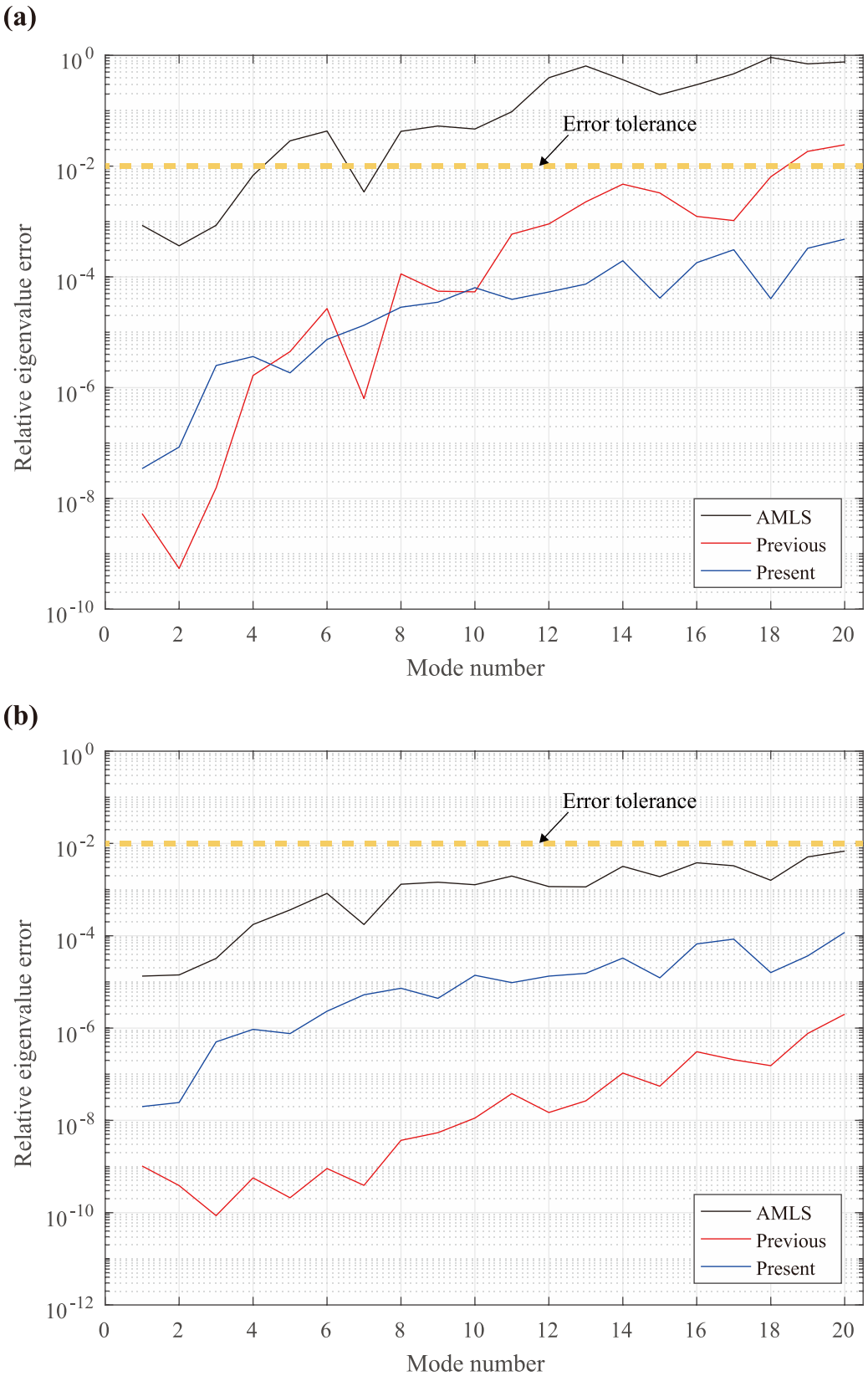

Figure 5.2 Relative eigenvalue errors for the rectangular plate problem: (a) Case A, (b) Case B

Table 5.1 Relative eigenvalue errors for the rectangular plate problem in Case A

Mode number	AMLS	EAMLS	
		Previous	Present
1	8.54038×10^{-4}	5.31416×10^{-9}	3.43342×10^{-8}
2	3.64345×10^{-4}	5.43980×10^{-10}	8.43386×10^{-8}
3	8.52799×10^{-4}	1.55100×10^{-8}	2.50882×10^{-6}
4	6.81176×10^{-3}	1.65724×10^{-6}	3.64546×10^{-6}
5	2.86210×10^{-2}	4.47137×10^{-6}	1.85045×10^{-6}
6	4.30107×10^{-2}	2.68323×10^{-5}	7.40431×10^{-6}
7	3.41986×10^{-3}	6.34895×10^{-7}	1.33956×10^{-5}
8	4.24908×10^{-2}	1.13308×10^{-4}	2.83256×10^{-5}
9	5.29423×10^{-2}	5.50996×10^{-5}	3.48417×10^{-5}
10	4.67332×10^{-2}	5.37409×10^{-5}	6.38754×10^{-5}
11	9.62249×10^{-2}	5.90782×10^{-4}	3.92355×10^{-5}
12	3.94315×10^{-1}	9.04083×10^{-4}	5.33350×10^{-5}
13	6.43190×10^{-1}	2.26478×10^{-3}	7.42547×10^{-5}
14	3.63637×10^{-1}	4.72177×10^{-3}	1.95644×10^{-4}
15	1.95130×10^{-1}	3.27608×10^{-3}	4.13647×10^{-5}
16	2.95617×10^{-1}	1.23627×10^{-3}	1.80371×10^{-4}
17	4.64452×10^{-1}	1.03832×10^{-3}	3.09585×10^{-4}
18	9.18239×10^{-1}	6.41150×10^{-2}	4.04529×10^{-5}
19	7.00959×10^{-1}	1.84309×10^{-2}	3.28335×10^{-4}
20	7.62391×10^{-1}	2.42997×10^{-2}	4.79123×10^{-4}

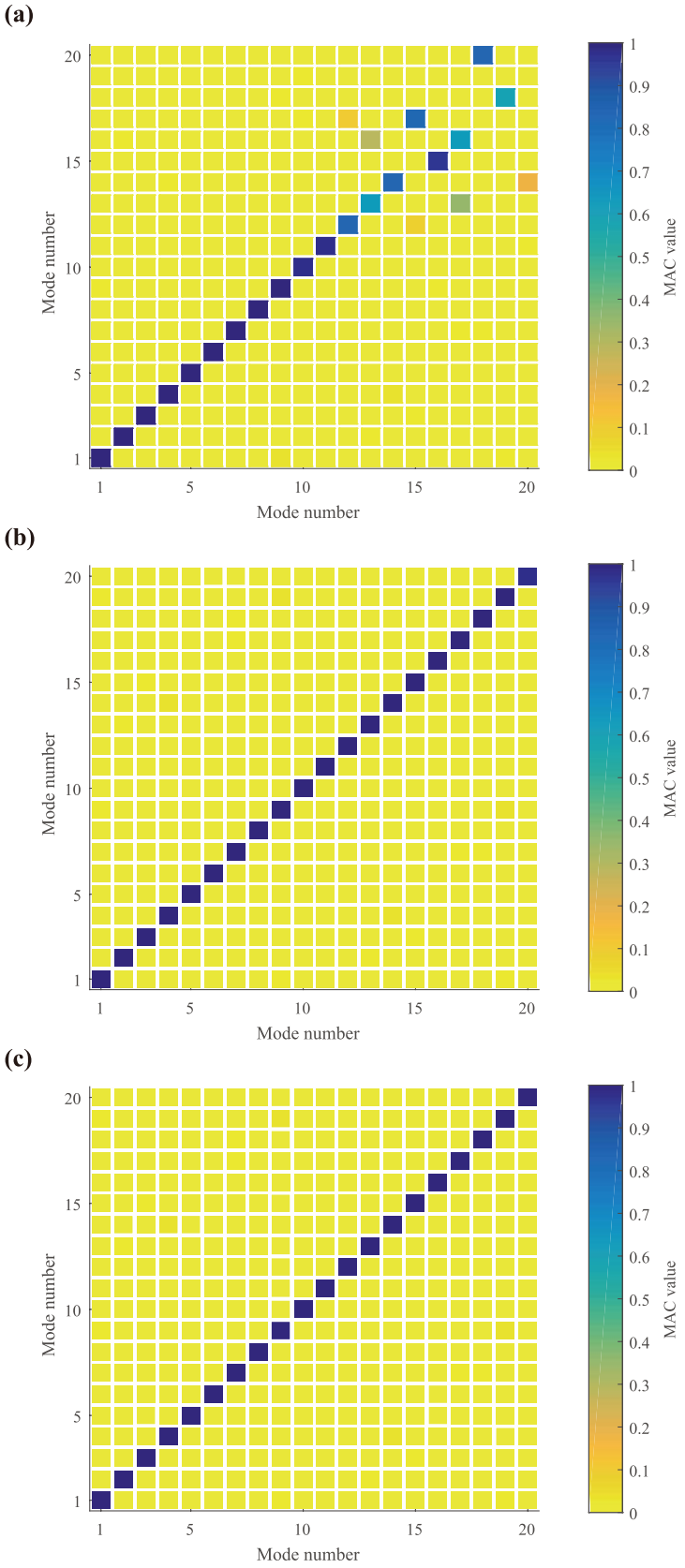

Figure 5.3 2-D presentation of MAC values for the rectangular plate problem in Case A: (a) AMLS, (b) previous EAMLS, (c) present EAMLS

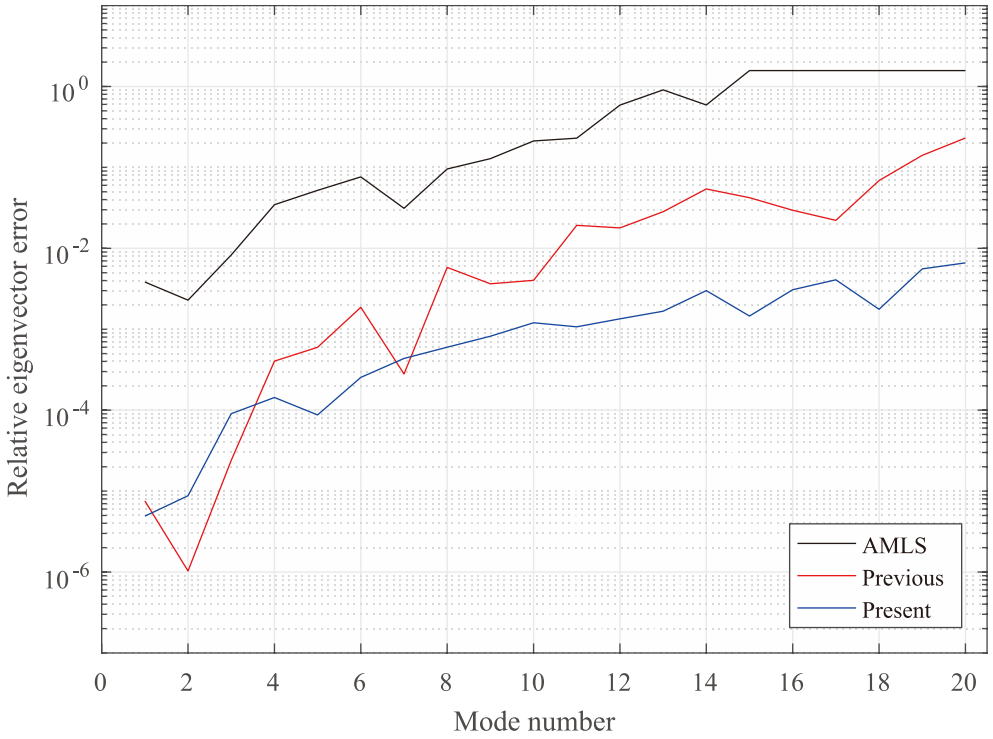

Figure 5.4 Relative eigenvector errors for the rectangular plate problem in Case A

Table 5.2 Specific computational cost for the rectangular plate problem in Case A

Methods	Items	Computation times	
		[sec]	Ratio [%]
AMLS	Calculation of constraint modes	0.11	12.09
	Transformation procedure	0.30	32.97
	Reduced eigenvalue problem	0.15	16.48
	Construction of transformation matrix	0.25	27.47
	Back transformation procedure	0.10	10.99
	Total	0.91	100.00
Previous EAMLS	Calculation of constraint modes and residual flexibility matrix	0.31	34.07
	AMLS transformation procedure	0.28	30.77
	Construction of extended constraint modes matrix	0.47	51.65
	Construction of the enhanced transformation matrix	2.05	225.27
	Reduced eigenvalue problem	0.15	16.48
	Back transformation procedure	0.01	1.10
	Total	3.27	359.34
Present EAMLS	Preliminary transformation procedure	0.41	45.06
	Projection on the refined subspace	0.01	1.10
	Residual substructural modes correction	0.09	9.89
	Reduced eigenvalue problem	0.14	15.38
	Construction of the enhanced transformation matrix	0.20	21.98
	Back transformation procedure	0.10	10.99
	Total	0.95	104.40

Table 5.3 Computational cost for the rectangular plate problem in Case B

Methods	Computation times	
	[sec]	Ratio [%]
AMLS	0.930	100.00
Previous EAMLS	3.528	379.35
Present EAMLS	0.996	107.10

5.2 Centrifugal impeller problem

Here, a centrifugal impeller, a key component of centrifugal compressor, is considered as shown in Figure 5.5. The impeller is modeled using 66201 four-node tetrahedral elements and the number of total DOFs is 52332. Young's modulus E is 207 GPa, Poisson's ratio ν is 0.3, and density ρ is 7850 kg/m^3. The reduced models obtained from the AMLS, previous and present EAMLS are constructed in the same size.

The global mass and stiffness matrices for the AMLS, previous and present EAMLS methods are partitioined 322 substructures using algebraic substructuring. For AMLS and previous EAMLS methods, the number of DOFs of the reduced bottom and higher level substructures are 162 and 1415, respectively. For present method to construct the same DOFs of reduced model, the number of DOFs of the reduced bottom level substructure and extended root substructure are 194 and 1383, respectively. Therefore, the number of DOFs of reduced models are 1577.

Figure 5.6, 5.7, and 5.8 illustrate the relative eigenvalue errors, MAC values, and relative eigenvector errors computed by the AMLS, previous and present EAMLS methods up to the 60^{th} mode, respectively. Table 5.4 lists the required computational costs for each method. As aforementioned in chapter 3 and 4, computation of enhanced transformation by global operation is identified as bottleneck in the previous EAMLS method. In addition, explicit calculation of substructural residual flexibility matrix $\mathbf{F}_i^{rs}$, fully populated matrices, is required large computer memory and gives rise to additional arithmetic operations.

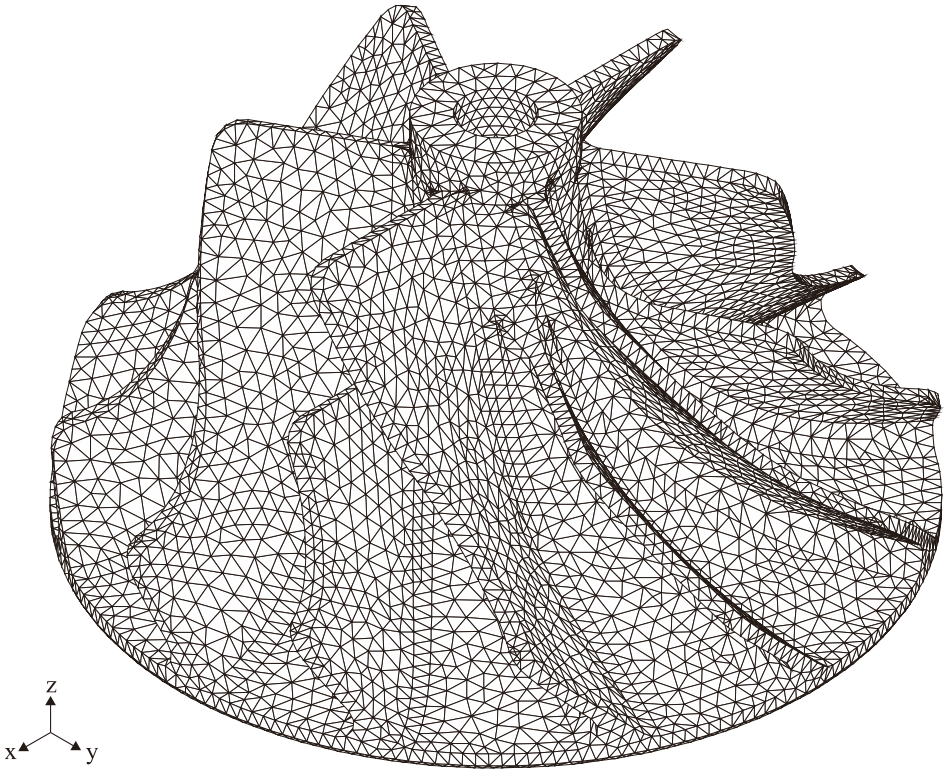

Figure 5.5 A centrifugal impeller model

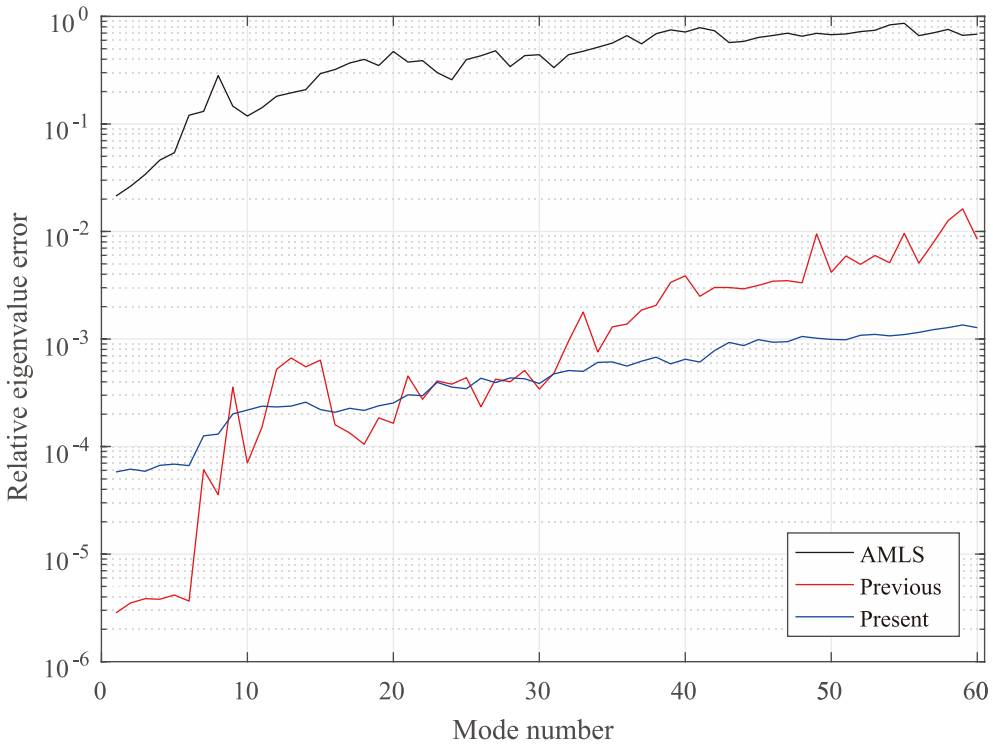

Figure 5.6 Relative eigenvalue errors for the centrifugal impeller problem

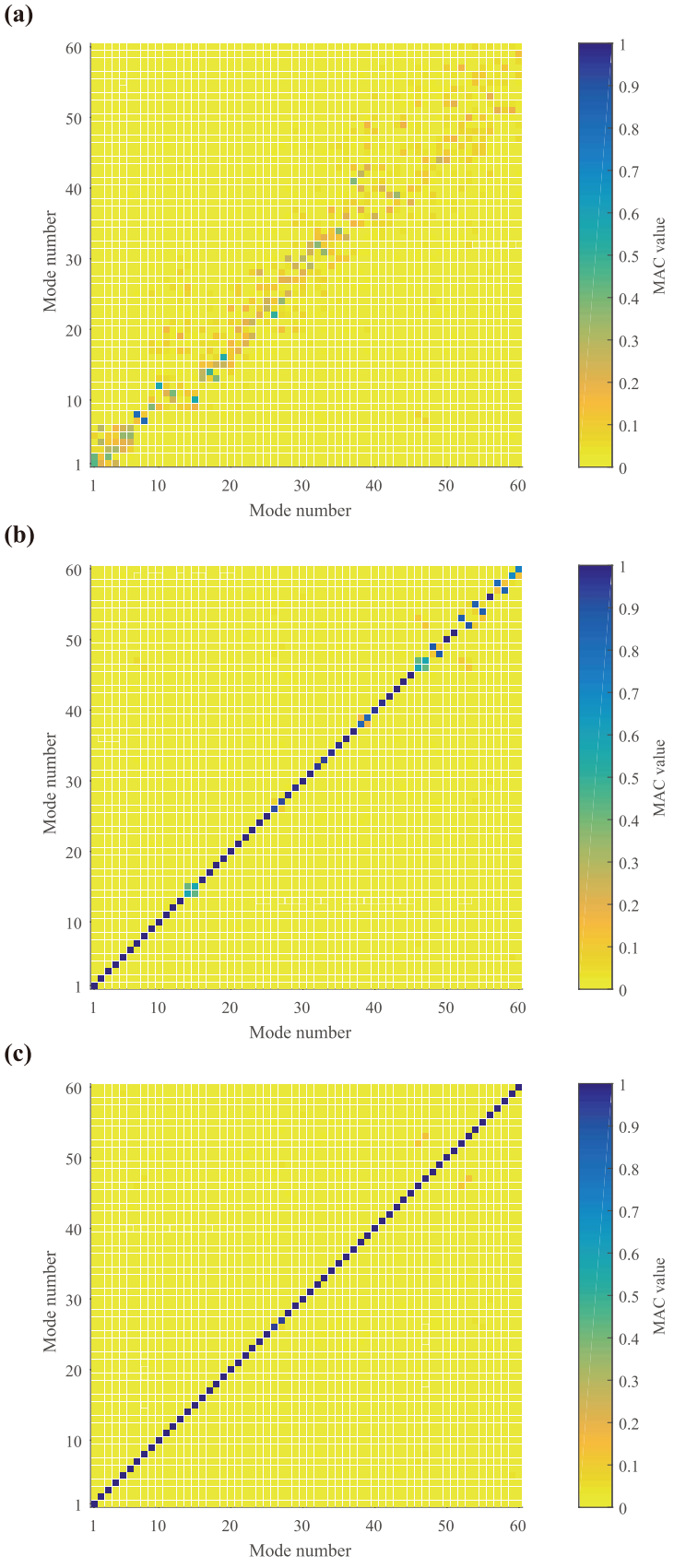

Figure 5.7 2-D presentation of MAC values for the centrifugal impeller problem: (a) AMLS, (b) previous EAMLS, (c) present EAMLS

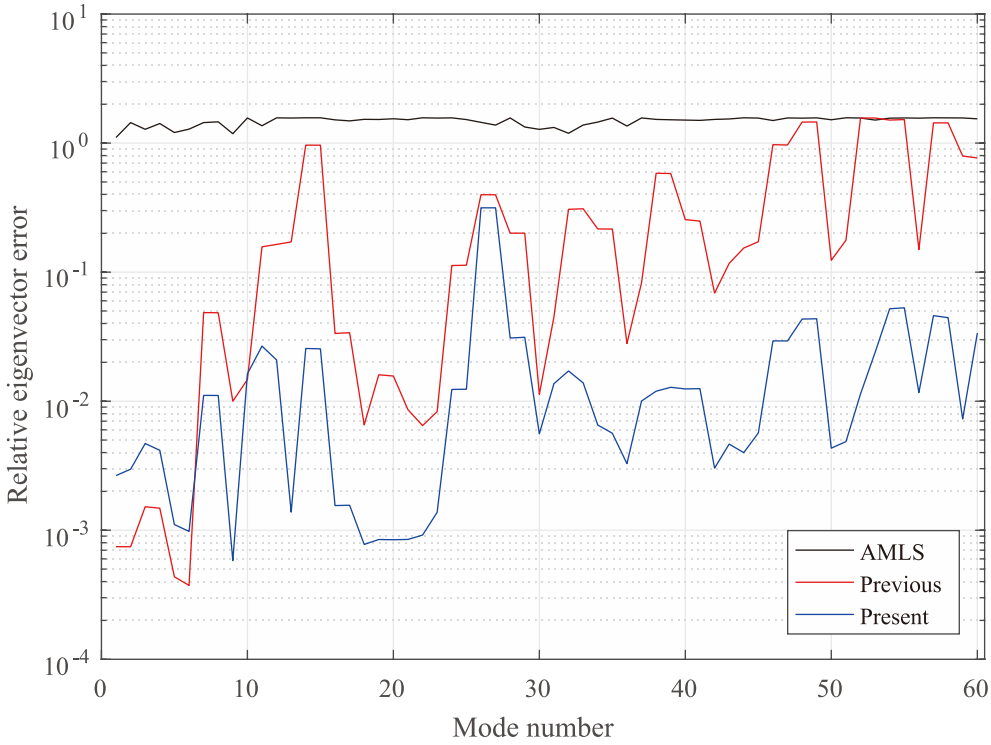

Figure 5.8 Relative eigenvector errors for the centrifugal impeller problem

Table 5.4 Specific computational cost for the centrifugal impeller problem

Methods	Items	Computation times	
		[sec]	Ratio [%]
AMLS	Calculation of constraint modes	2.95	4.28
	Transformation procedure	55.66	80.80
	Reduced eigenvalue problem	0.87	1.26
	Construction of transformation matrix	9.08	13.18
	Back transformation procedure	0.33	0.48
	Total	68.89	100.00
Previous EAMLS	Calculation of constraint modes and residual flexibility matrix	4.39	6.37
	AMLS transformation procedure	59.93	86.99
	Construction of extended constraint modes matrix	64.62	93.80
	Construction of the enhanced transformation matrix	3015.17	4376.79
	Reduced eigenvalue problem	1.62	2.35
	Back transformation procedure	0.25	0.36
	Total	3145.98	4566.67
Present EAMLS	Preliminary transformation procedure	59.27	86.03
	Projection on refined subspace	1.68	2.44
	Residual substructural modes correction	9.65	14.01
	Reduced eigenvalue problem	0.77	1.12
	Construction of the enhanced transformation matrix	2.76	4.01
	Back transformation procedure	1.36	1.97
	Total	75.49	109.58

5.3 Femur bone problem

Over the past few decades, FE analysis has been applied for simulating biomedical engineering systems to predict the dynamic properties such as natural frequencies, vibration modes, and fracture load. Here, a femur bone is considered as shown in Figure 5.9. The bone material is inherently anisotropic, but is assumed to be isotropic material. Young's modulus E is 18 GPa, Poisson's ratio ν is 0.3, and density ρ is 1900 kg/m^3 [42]. For modeling the femur bone, 425345 four-node tetrahedral element are used, and the number of DOFs is 289431. In this problem, the reduced models cannot be obtained from the previous EAMLS method since direct calculation of the enhanced transformation matrix is required large computational memory and time. The global mass and stiffness matrices are partitioned into 997 substructures for both methods using algebraic substructuring, and the reduced model obtained by AMLS and present EAMLS methods are constructed in the same size.

For the AMLS method, the number of DOFs of the reduced bottom and higher level substructures are 499 and 1167. For the present method, the number of DOFs of the reduced bottom level substructures and extended root substructure are 1466 and 200, respectively. Therefore, the number of DOFs of reduced models are 1666. Figure 5.10 represents the relative eigenvalue errors corresponding to $1^{st} \sim 100^{th}$ and Table 5.5 shows computational cost obtained from AMLS and present method. These results demonstrates the excellent solution accuracy and only required slight additional computational cost compared to AMLS method.

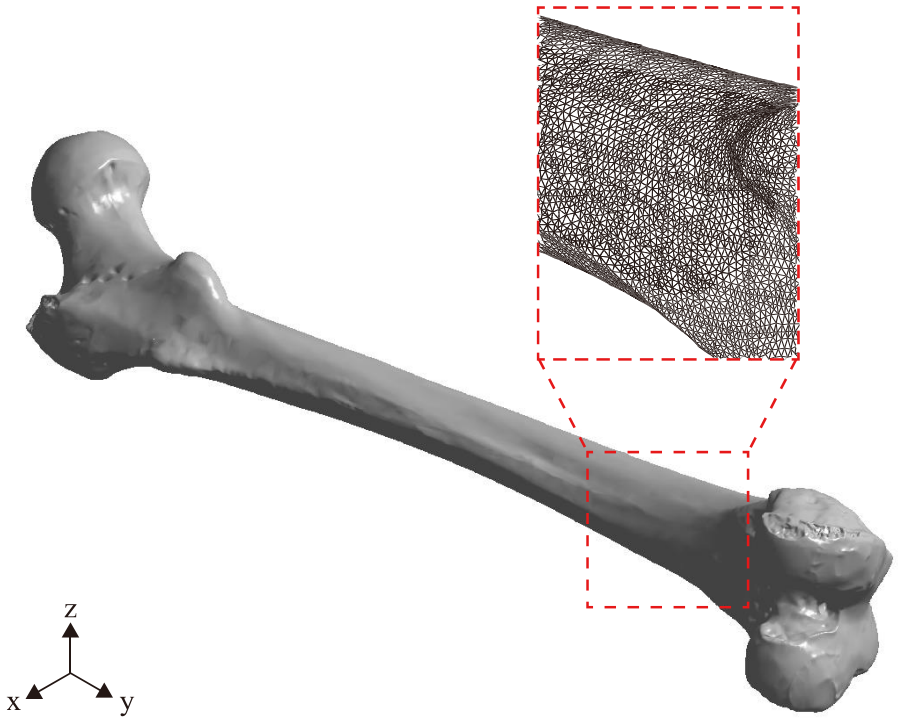

Figure 5.9 A femur bone model

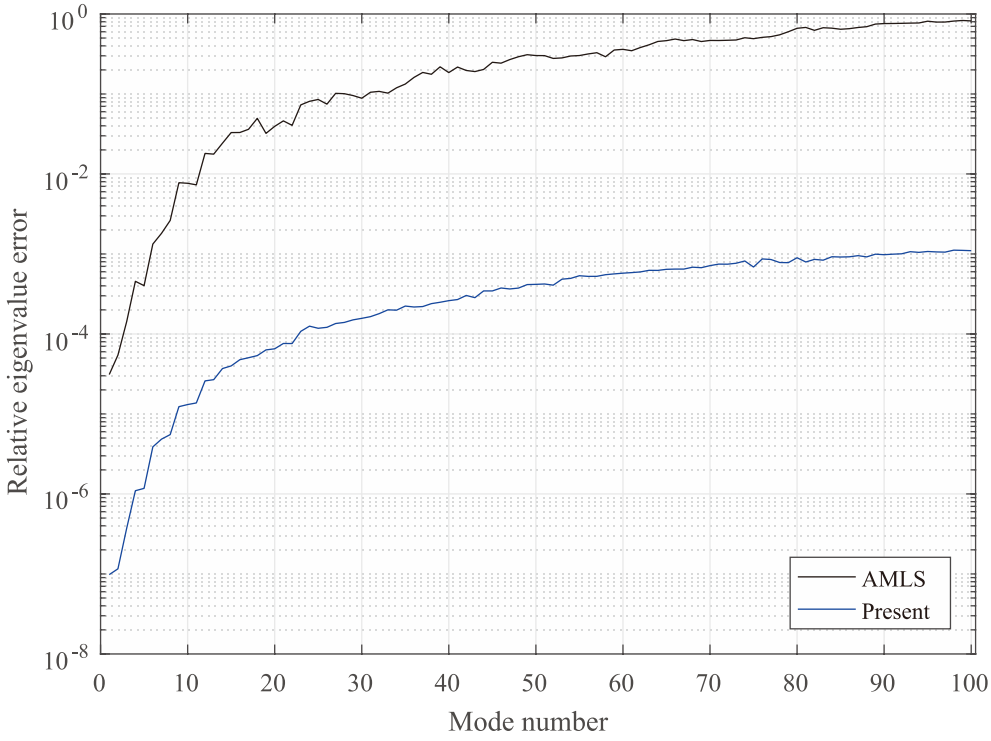

Figure 5.10 Relative eigenvalue errors for the femur bone prblem

Table 5.5 Computational cost for the femur bone problem

Methods	Computation times	
	[sec]	Ratio [%]
AMLS	627.17	100.00
Previous EAMLS	N/A	-
Present EAMLS	707.92	112.88

5.4 Airplane fuselage problem

Here, an airplane fuselage, modeled by three-node shell element, is considered as shown in Figure 5.11 to validate the performance of present method for relatively large FE model. Young's modulus E is 71 GPa, Poisson's ratio ν is 0.3, and density ρ is 2770 kg/m^3. The number of element and DOFs in global FE model are 675056 and 2025180, respectively. In this problem, the reduced model cannot be obtained from previous EAMLS method like femur bone problem. The global FE model is partitioned into 6112 substructures for both methods using algebraic substructuring.

In order to compare the efficiency between AMLS and present EAMLS methods at similar accuracy, the sizes of the reduced model are different. Figure 5.12 illustrates the relative eigenvalue errors up to 300^{th} mode from the four different DOFs of reduced models: $\overline{N} = 21802$, $\overline{N} = 26561$, $\overline{N} = 31655$, and $\widetilde{N} = 3784$. Total computational costs are listed in the Table 5.6. From these results, the present method can construct a small size reduced model with better efficiency compared to the AMLS method.

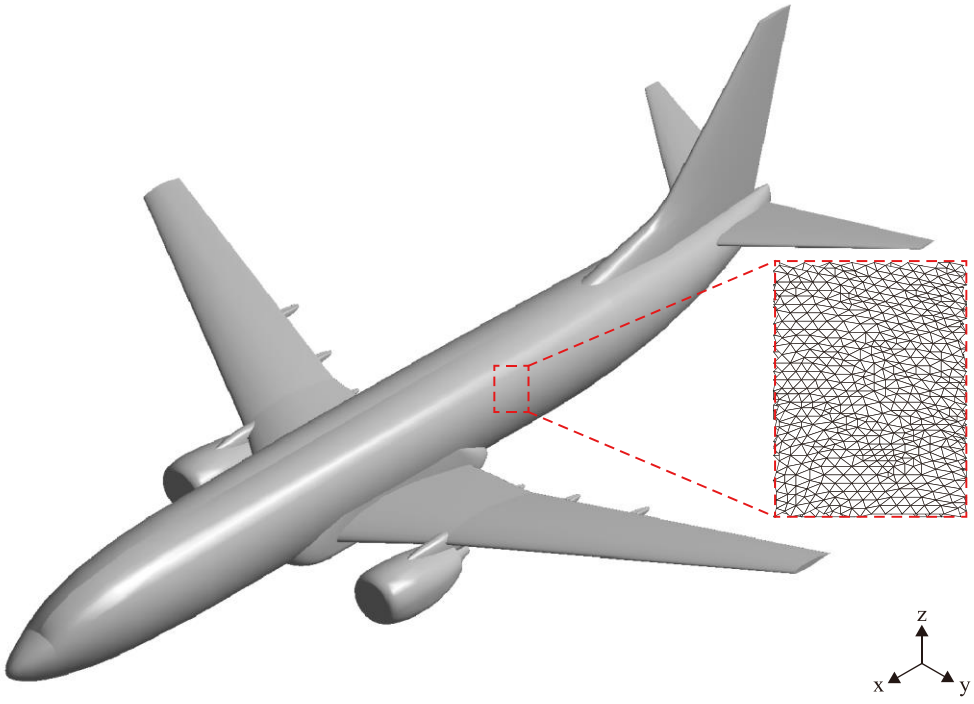

Figure 5.11 An airplane fuselage model

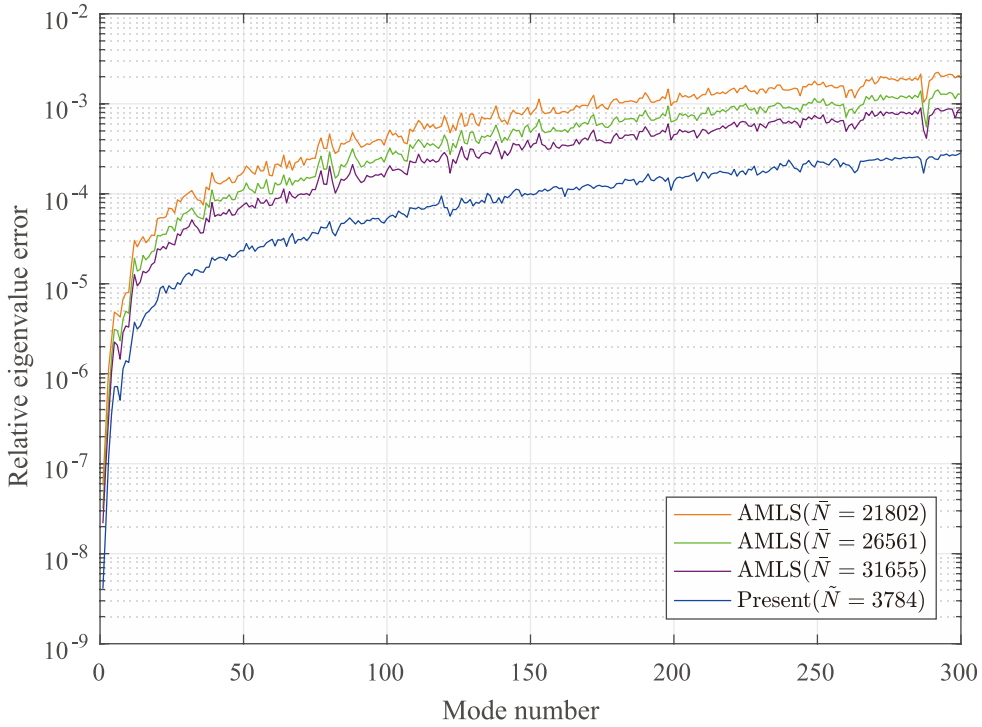

Figure 5.12 Relative eigenvalue errors for the airplane fuselage problem

Table 5.6 Computational cost for the airplane fuselage problem

Methods		Computation times	
		[sec]	Ratio [%]
AMLS	($\bar{N}$ = 21802)	5705.36	95.07
AMLS	($\bar{N}$ = 26561)	5889.58	98.14
AMLS	($\bar{N}$ = 31655)	6001.23	100.00
Previous EAMLS		N/A	-
Present EAMLS	($\tilde{N}$ = 3784)	5600.41	93.32

Chapter 6. Conclusions

In this thesis, the new formulation of EAMLS method for reduction of the large FE models has been presented. In order to resolve the factors associated with deteriorating efficiency, three phases for managing the computer memory and computational cost were discussed in detailed: algebraic substructuring with reverse level order traversal, projection on the refined subspace, and the residual substructural modes correction. The new formulation employed these processes represents the extremely increase efficiency compared to the previous EAMLS method and has capability to solve the large and complex models over millions DOFs. Unlike the previous EAMLS method, residual flexibility matrices is derived from only bottom level substructures and not required explicitly. In addition, residual substructural modes correction is applied to only the mass matrix, and this give rise to an efficient algorithm. The new formulation is demonstrated its accuracy and efficiency through various numerical examples, and identified to enable reduction of large and complex FE models which cannot be solved from the previous EAMLS method.

In the future work, it would be possible to develop a more robust EAMLS method with efficient mode selection, which has a significant on both accuracy and computational cost. For this, it should be investigated the effect of the selected modes and optimal choice of modes.

Appendix

Table A.1 lists the reference eigenvalues λ for the rectangular plate problem in Section 5.1 up to 30^{th} mode.

Table A.1 The reference eigenvalues for the rectangular plate problem in Section 5.1

Mode number	Reference λ
1	-9.35828×10^{-10}
2	1.65559×10^{-9}
3	4.24917×10^{-9}
4	4.87676×10^{-9}
5	5.90795×10^{-9}
6	6.57825×10^{-9}
7	0.696479971
8	0.749201188
9	3.842803708
10	5.341551279
11	5.732317012
12	9.101727949
13	12.60505321
14	18.82903417
15	22.78273281
16	33.69775915
17	40.95263798
18	45.13653716
19	50.81684223
20	62.03892043
21	74.84707080
22	80.81029884
23	81.28972606
24	118.6988289
25	141.4146650
26	149.6863495
27	168.3535584
28	176.3333556
29	188.0154359
30	190.6058926

Bibliography

[1] K.J. Bathe, Finite element procedures, Prentice Hall, USA, 1996.

[2] R.J. Guyan, Reduction of stiffness and mass matrices, AIAA J. 3 (1965) 380–380.

[3] B. Irons, Structural eigenvalue problems - elimination of unwanted variables, AIAA J. 3 (1965) 961–962.

[4] J. O'Callahan, A procedure for an improved reduced system (IRS) model, Proceedings of the 7th international modal analysis conference, Las Vegas, 1 (1989) 17-21.

[5] M.I. Friswell, S.D. Garvey, J.E.T. Penny, Model reduction using dynamic and iterated IRS techniques, J. Sound Vib. 186 (1995) 311–323.

[6] Z.Q. Qu, Z.F. Fu, New Structural Dynamic Condensation Method for Finite Element Models, AIAA J. 36 (1998) 1320–1324.

[7] Y. Xia, R.-M. Lin, Improvement on the iterated IRS method for structural eigensolutions, J. Sound Vib. 270 (2004) 713–727.

[8] H. Kim, M. Cho, Improvement of reduction method combined with sub-domain scheme in large-scale problem, Int. J. Numer. Methods Eng. 70 (2007) 206–251.

[9] S.H. Boo, P.S. Lee, A dynamic condensation method using algebraic substructuring, Int. J. Numer. Methods Eng. 109 (2017) 1701–1720.

[10] S.H. Boo, P.S. Lee, An iterative algebraic dynamic condensation method and its performance, Comput. Struct. 182 (2017) 419–429.

[11] W.C. Hurty, Dynamic analysis of structural systems using component modes, AIAA J. 3 (1965) 678–685.

[12] R.R. Craig, M.C.C. Bampton, Coupling of Substructures for Dynamics Analyses, AIAA J. 6 (1968) 1313.

[13] R.L. Goldman, Vibration analysis by dynamic partitioning., AIAA J. 7 (1969) 1152–1154.

[14] R.M. Hintz, Analytical Methods in Component Modal Synthesis, AIAA J. 13 (1975) 1007–1016.

[15] J.K. Bennighof, M.F. Kaplan, Frequency sweep analysis using multi-level substructuring, global modes and iteration, 39th AIAA/ASME/ASCE/AHS/ASC Struct. Struct. Dyn. Mater. Conf. Exhib., Long Beach, CA, 1998.

[16] M.F. Kaplan, Implementation of automated multilevel substructuring for frequency response analysis of structures, Ph.D. thesis, Department of Aerospace Engineering & Engineering Mechanics, University of Texas, Austin TX, 2001.

[17] J.K. Bennighof, R.B. Lehoucq, An Automated Multilevel Substructuring Method for Eigenspace Computation in Linear Elastodynamics, SIAM J. Sci. Comput. 25(6) (2004) 2084-2106.

[18] K.C. Park, Y.H. Park, Partitioned Component Mode Synthesis via a Flexibility Approach, AIAA J. 42 (2004) 1236–1245.

[19] D.J. Rixen, A dual Craig-Bampton method for dynamic substructuring, J. Comput. Appl. Math. 168 (2004) 383–391.

[20] M. Kim, An Efficient Eigensolution Method and Its Implementation for Large Structural Systems, Ph.D. thesis, Department of Aerospace Engineering & Engineering Mechanics, University of Texas, Austin TX, 2004.

[21] C. Yang, W. Gao, Z. Bai, X.S. Li, L.Q. Lee, P. Husbands, E. Ng, An Algebraic Substructuring Method for Large-Scale Eigenvalue Calculation, SIAM J. Sci. Comput. 27 (2005) 873–892.

[22] K. Elssel, H. Voss, An A Priori Bound for Automated Multilevel Substructuring, SIAM J. Matrix Anal. Appl. 28 (2006) 386–397.

[23] S. Baek, M. Cho, The transient and frequency response analysis using the multi-level system condensation in the large-scaled structural dynamic problem, Struct. Eng. Mech. 38 (2011) 429–441.

[24] J. Yin, H. Voss, P. Chen, Improving eigenpairs of automated multilevel substructuring with subspace iterations, Comput. Struct. 119 (2013) 115–124.

[25] J.G. Kim, P.S. Lee, An enhanced Craig-Bampton method, Int. J. Numer. Methods Eng. 103 (2015) 79–93.

[26] J.G. Kim, S.H. Boo, P.S. Lee, An enhanced AMLS method and its performance, Comput. Methods Appl. Mech. Eng. 287 (2015) 90–111.

[27] S.H. Boo, J.G. Kim, P.S. Lee, A simplified error estimator for the CB method and its application to error control, Comput. Struct. 164 (2016) 53–62.

[28] S.H. Boo, J.G. Kim, P.S. Lee, Error estimation for the automated multi-level substructuring method, Int. J. Numer. Methods Eng. 106 (2016) 927–950.

[29] J.H. Kim, J. Kim, P.S. Lee, Improving the accuracy of the dual Craig-Bampton method, Comput. Struct. 191 (2017) 22–32.

[30] A. Kropp, D. Heiserer, Efficient broadband vibro-acoustic analysis of passenger car bodies using an FE-based component mode synthesis approach, J. Comput. Acoust. 11 (2003) 139–157.

[31] C. Yang, W. Gao, Z. Bai, X.S. Li, L.Q. Lee, P. Husbands, E.G. Ng, Algebraic Sub-structuring for Electromagnetic Applications, Lect. Notes. Comput. Sci. 3732 (2006) 364-373.

[32] W. Rachowicz, A. Zdunek, Automated multi-level substructuring (AMLS) for electromagnetics, Comput. Methods Appl. Mech. Eng. 198 (2009) 1224–1234.

[33] Y. Xia, R. Lin, A new iterative order reduction (IOR) method for eigensolutions of large structures, Int. J. Numer. Methods Eng. 59 (2004) 153–172.

[34] R.H. MacNeal, A hybrid method of component mode synthesis, Comput. Struct. 1 (1971) 581–601.

[35] G. Masson, B. Ait Brik, S. Cogan, N. Bouhaddi, Component mode synthesis (CMS) based on an enriched ritz approach for efficient structural optimization, J. Sound Vib. 296 (2006) 845–860.

[36] R.J. Kuether, M.S. Allen, Craig-bampton substructuring for geometrically nonlinear subcomponents, Conf. Proc. Soc. Exp. Mech. Ser. 1 (2014) 167–178.

[37] A. George, Nested Dissection of a Regular Finite Element Mesh, SIAM J. Numer. Anal. 10 (1973) 345–363.

[38] G. Karypis, V. Kumar, A Fast and High Quality Multilevel Scheme for Partitioning Irregular Graphs, SIAM J. Sci. Comput. 20 (1998) 359–392.

[39] A. Drozdek, Data structures and algorithms in C++, 2005.

[40] O.E. Hansteen, K. Bell, On the accuracy of mode superposition analysis in structural dynamics, Earthq. Eng. Struct. Dyn. 7 (1979) 405–411.

[41] E.N. Dvorkin, K. Bathe, A continuum mechanics based four-node shell element for general non-linear analysis, Eng. Comput. 1 (1984) 77–88.

[42] R.B. Ashman, S.C. Cowin, W.C. Van Buskirk, J.C. Rice, A continuous wave technique for the measurement of the elastic properties of cortical bone, J. Biomech. 17 (1984) 349–361.